

UNIVERSITY OF HELSINKI
REPORT SERIES IN PHYSICS

HU-P-D231

THE USE OF MOSFET DOSIMETERS AND ANTHROPOMORPHIC PHANTOMS IN LOW DOSE DENTAL CBCT APPLICATIONS

Juha Koivisto

Department of Physics
Faculty of Science
University of Helsinki
Helsinki, Finland

ACADEMIC DISSERTATION FOR THE DEGREE OF DOCTOR OF PHILOSOPHY

To be presented, with the permission of the Faculty of Science of the University of Helsinki,
for public examination in Auditorium XII, University Main Building, (Fabianinkatu 33),
on the 16th of October 2015 at 12 noon.

HELSINKI 2015

SUPERVISED BY

Sauli Savolainen, PhD, Professor
HUS Medical Imaging Center,
University of Helsinki, Finland

Mika Kortnesniemi, PhD, Adjunct Professor
HUS Medical Imaging Center,
University of Helsinki, Finland

Jan Wolff, Dr. med. dent., Assistant Professor
Department of Oral and Maxillofacial Surgery,
VU University Medical Center, Amsterdam, The Netherlands

PRE-EXAMINED BY

Miika Nieminen, PhD, Professor,
University of Oulu, Finland

and

Simo Saarakkala, PhD, Associate Professor,
University of Oulu, Finland

OPPONENT

Juha Nikkinen, PhD, Associate Professor,
University of Oulu, Finland

© 2015 Juha Koivisto

ISSN 0356-0961
ISBN 978-951-51-0595-0 (pbk.)
Helsinki University Print
Helsinki 2015

ISBN 978-951-51-0596-7 (PDF)
Helsinki University E-thesis
<http://ethesis.helsinki.fi>
Helsinki, 2015

ABSTRACT

The growing number of x-ray examinations being routinely performed on patients using cone-beam computed tomography (CBCT) and multi-slice computed tomography (MSCT) devices have led to an emerging risk of and concern about radiation exposure. Typical CBCT absorbed doses range between 1–7 mGy, and thus values less than 1 mGy can be considered as low dose values. To date, most studies concerning effective dose assessment in the maxillofacial region use anthropomorphic phantoms in combination with thermoluminescent dosimeters (TLD). Recently, MOSFET dosimeters have been considered as a possible alternative to TLDs for in vitro dose assessment. The major benefit of MOSFET dosimeters is their real-time dose measurement capabilities.

All 20 MOSFET dosimeters were characterized for CBCT photon energy ranges, dose properties, and organ dose measurements using TLD dosimeters (I). The MOSFET dosimeter energy dependencies were evaluated for two photon energy ranges in order to encompass the typical mean photon energies used in dental radiology. Furthermore, the MOSFET dosimeter uncertainty was assessed by repetitive measurements at different doses. The MOSFET angular sensitivity was investigated using dental photon energies and soft tissue equivalent backscatter material. After MOSFET characterization, a dose measurement setup was developed. The setup comprised 20 MOSFET dosimeters that were placed into the allocated grid holes of an anthropomorphic RANDO phantom. The MOSFET dose measurement setup was validated using two different methods: Monte Carlo simulations and TLD dosimeters. The setup was used for organ and effective dose assessments resulting from supine, prone, and oblique phantom positions in the maxillofacial region using a novel cone beam computed tomography (CBCT) device and from two conventional dental CBCTs and one multi-slice computed tomography (MSCT) device.

All MOSFET dosimeters demonstrated a statistically insignificant energy dependency when using typical dental photon energies. Furthermore, the MOSFETs demonstrated excellent dose linearity and resulted in similar absorbed organ doses to those attained in the TLD measurements. The required low dose limit was achieved by averaging the values attained using eight MOSFET exposures. The MOSFET dosimeter angular dependency demonstrated a 5% standard deviation from the mean sensitivity value. The MOSFET dose assessment setup demonstrated similar effective doses to those attained using the Monte Carlo simulations and TLD measurements. Effective dose was strongly dependent on the vertical phantom positioning and minor vertical changes resulted in dose increases of up to 16%. The dose measurements acquired using the same FOV on all CBCT and MSCT devices

resulted in the following values: Planmed Verity CBCT scanner 247 μSv in supine, 192 μSv in prone, and 134 μSv in oblique position, the ProMax 3D MAX CBCT 168 μSv , i-CAT Next Generation 170 μSv , Philips Brilliance 64 MSCT 781 μSv .

The results of this study demonstrate that the mean photon energy dose dependency corrections are not required in typical dental energy ranges. Furthermore, averaging eight MOSFET exposures attained typical TLD low dose values. Due to their variation in angular sensitivity, MOSFET dosimeters should always be calibrated in clinical settings for beam geometry and the angular range of the CBCT exposure. Based on the results of the Monte Carlo simulations and TLD measurements, the MOSFET measurement setup constitutes a feasible method for low dose assessment in CBCT and MSCT devices in the maxillofacial region. When using the same FOV and exposure parameters, the effective doses obtained in the supine position were 29% higher (247 μSv) than those obtained in the prone position (192 μSv). When the prone and oblique positions were compared, the observed effective dose in the oblique position was 30% lower. Thus, optimal patient positioning can reduce the dose and subsequently minimize the radiation risks. In summary, the fast and dependable low- dose measurement setup presented in this thesis provides an effective means of CBCT dose assessment using a variety of exposure parameters, patient positioning, and FOVs. Further, the setup presented in this study can be used to test and develop CBCT devices that would subsequently produce lower effective doses. Since radiologists commonly only have access to the radiation output of different devices, they lack the possibility to assess the actual effective dose. Therefore, the setup developed in this thesis can also be utilized to increase the awareness of the lifetime radiation risks amongst radiologists leading to dose reduction

TABLE OF CONTENTS

ABSTRACT	3
LIST OF ORIGINAL PUBLICATIONS	7
AUTHOR'S CONTRIBUTIONS.....	8
LIST OF ABBREVIATIONS AND SYMBOLS	9
1 INTRODUCTION	12
1.1 Radiation from x-ray sources	12
1.2 CBCT technology.....	13
1.3 Dosimeters and dose assessment methods	14
2 AIMS AND STRUCTURE OF THE THESIS.....	17
3 MATERIALS AND METHODS	19
3.1. Dosimeters	19
3.1.1 MOSFET dosimeters	19
3.1.2. Reference dosimeters	20
3.2. Characterization of MOSFET dosimeters	21
3.2.1. Photon energy dependency	21
3.2.2. Dose, dose rate, and accumulated dose dependencies	23
3.2.3. Angular dependency	24
3.2.4. MOSFET dosimeter uncertainty	26
3.3. Head phantom used for effective dose assessment.....	27
3.4 Equivalent and effective dose assessment.....	28
3.5. MOSFET setup used for effective dose assessment.....	30
3.6. Validation of the MOSFET dose measurement method.....	31
3.6.1. Effective doses determined using MOSFETs and Monte Carlo simulations.....	31
3.6.2. MOSFET and TLD comparisons.....	33
3.7. MOSFET dose measurement setup application.....	35
3.8. Effective dose uncertainties	36

4	RESULTS	37
4.1.	Characterization of MOSFET dosimeters	37
4.1.1.	Photon energy dependency	37
4.1.2.	Dose, dose rate, and accumulated dose dependencies.....	38
4.1.3.	Angular dependency.....	38
4.1.4.	MOSFET dosimeter uncertainty	39
4.2.	Validation of MOSFET dose measurement method	40
4.2.1.	MOSFET measurements and Monte Carlo simulations.....	40
4.2.2.	MOSFET and TLD comparisons	43
4.3.	Effective doses obtained using one MDCT device and three CBCT devices	44
4.4.	Effective dose uncertainties.....	45
5	DISCUSSION.....	46
5.1	MOSFET dosimeter characterization for dose dependencies.....	47
5.2.	MOSFET dosimeter uncertainty.....	48
5.3.	Validation of the MOSFET dose measurement setup.....	49
5.4.	MOSFET dose measurement setup application.....	51
5.5.	Future developments in effective dose assessment	52
6	CONCLUSIONS.....	54
7	ACKNOWLEDGEMENTS.....	55
	REFERENCES	56

LIST OF ORIGINAL PUBLICATIONS

The thesis is based on the following original publications referred to in the text by their Roman numerals.

- I Koivisto J, Wolf J, Kiljunen T, Schulze D, Kortnesniemi M. “*Characterization of MOSFET dosimeters for low-dose measurements in maxillofacial anthropomorphic phantoms*”. **J Appl Clin Med Phys.** 2015 Jul 8;16(4):5433.
- II Koivisto J, Kiljunen T, Wolf J, Kortnesniemi M. “*Characterization of MOSFET dosimeter angular dependence in three rotational axes measured free-in-air and in soft-tissue equivalent material*”. **Journal of Radiation Research,** 2013, 00, 1–7 doi: 10.1093/jrr/rrt015
- III Koivisto J, Kiljunen T, Tapiovaara M, Wolff J, Kortnesniemi M. “*Assessment of radiation exposure in dental cone-beam computerized tomography with the use of metal-oxide semiconductor field-effect transistor (MOSFET) dosimeters and Monte Carlo simulations*”. **Oral Surg Oral Med Oral Pathol Oral Radiol** 2012;114:393-400
- IV Koivisto J, Schulze D, Wolff J, Rottke D. “*Effective dose assessment in the maxillofacial region using thermoluminescent (TLD) and metal oxide semiconductor field- effect transistor (MOSFET) doseimeters: a comparative study*”. **Dentomaxillofac Radiol.** 2014;43(8):20140202. doi: 10.1259/dmfr.20140202. Epub 2014 Aug 21.
- V Koivisto J, Wolff J, Järnstedt J, Dastidar P, Kortnesniemi M. “*Assessment of the effective dose in supine, prone, and oblique positions in the maxillofacial region using a novel combined extremity and maxillofacial cone beam computed tomography scanner.*” **Oral Surg Oral Med Oral Pathol Oral Radiol.** 2014 Sep;118(3):355-62. doi: 10.1016/j.oooo.2014.05.016. Epub 2014 Jun 14.

AUTHOR'S CONTRIBUTIONS

Publication I

Review of the literature, research plan, experimental work on the characterization of MOSFET dosimeters for low dose measurements, analysis of the results, and writing the article.

Publication II

Review of the literature, design, realization of the measurement setup, measurements of angular dependency, analyzing the results, and writing the article.

Publication III

The development of a dose measurement setup that comprised MOSFET dosimeters and an anthropomorphic phantom designed to assess CBCT organ and effective doses from the maxillofacial region. Performing the measurements and mathematical simulations to obtain effective doses in the maxillofacial region. Validation of the method by comparing the results attained using simulation from a mathematical model, analyzing the results, and writing the article.

Publication IV

Performing the dose measurements in four different dental protocols using MOSFET dosimeters, collaborating with thermo luminescent dosimeter (TLD) dose measurements, validating the MOSFET measurement method using the results of the two different methods, analyzing the results, and writing the article.

Publication V

Implementing the effective measuring system to evaluate effective doses from the maxillofacial region for one MSCT and for three CBCT devices, analyzing the effective dose results, and writing the article.

The results of these studies have not been used in other Ph.D. studies.

LIST OF ABBREVIATIONS AND SYMBOLS

2D	Two-dimensional
3D	Three-dimensional
1SD	One standard deviation
2SD	Two standard deviations
ALARA	As low as reasonably achievable
CAT	Computerized axial tomography
CBCT	Cone beam computed tomography
cc	correlation coefficient
CT	Computed tomography
CTDI	Computed tomography dose index
D_{Ti}	Average absorbed dose of tissue T in layer i
<i>DAP</i>	Dose-area product
DLP	Dose-length product
<i>DT</i>	Absorbed tissue dose
FOV	Field of view
HVL	Half value layer
IAEA	International Atomic Energy Agency
IC	Ionization chamber
ICRP	International Commission on Radiation Protection

List of abbreviations and symbols

ICRU	International Commission on Radiation Unit and Measurements
IEC	International Electrotechnical Commission
Kerma	Kinetic energy released per unit mass
kVp	Peak kilovoltage
LNT	Linear no-threshold model
mAs	Product of tube current (mA) and exposure time (s)
MC	Monte Carlo
MSCT	Multi-slice computed tomography
MOSFET	Metal oxide semiconductor field effect transistor
MPD	multi-purpose detector
NRPB	National Radiological Protection Board
OSLD	optically stimulated luminescent dosimeter
PCXMC	PC based Monte Carlo program for calculating patient doses in medical X-ray examinations
PMMA	Polymethylmethacrylate
PSDL	Primary standard dosimetry laboratory
RANDO	Radiation Analogue Dosimetry system
RPLD	radio-photoluminescence dosimeters
SSDL	Secondary standard dosimetry laboratory
STUK	Finnish Radiation and Nuclear Safety Authority
T	Tissue
TLD	Thermoluminescent dosimeter
D	Absorbed organ dose

E	Effective dose
f_i	mass fraction of tissue T in layer i
H	Equivalent dose / radiation weighted dose
w_R	Radiation weighting factor
w_T	Tissue weighting factor

1 INTRODUCTION

1.1 RADIATION FROM X-RAY SOURCES

Since their discovery by Wilhelm Röntgen in November 1895, x-ray devices have provided undeniable benefits in clinical imaging. However, the negative affects of using ionizing radiation on patients were soon realized. In x-ray examinations, billions of photons pass through a patient during a single exposure, and increases the probability of causing alterations to the DNA of cells. In addition, it must be noted that according to the linear threshold model (LNT) (ICRP 103, 2008), even one radiation particle may be harmful and cause DNA mutations that can result in malignant tumors.

In order to minimize the lifetime radiation risks, both the number of examinations and the dose of each exposure should be reduced to the minimum and comply to the as low as reasonably achievable (ALARA) principle (ICRP 22, 1973). Additionally, one fundamental step in dose reduction is to develop measurement technologies that can reliably and effectively assess doses acquired during x-ray exposures. To date, the number of CBCT devices and subsequent imaging protocols is increasing, and several methods have been proposed to decrease the effective dose induced by CBCT devices. In the past, the most common method of reducing the dose induced by CBCT devices was to adjust the exposure parameters (Loubele 2008), (Ludlow 2008), (Suomalainen 2009), (Kau 2005) and more recently by using novel low-dose protocols (Xu 2012). The Health Protection Agency (HPA) Working Party has published guidelines on the safer use of CBCT devices (Holroyd 2010). Furthermore, the SEDENTEX Consortium (SEDENTEX 2011) and Pauwels et al. (Pauwels 2010) have published recommended effective dose ranges for CBCT devices. However, the number of exposures performed using low-dose CBCT devices worldwide is growing rapidly. Subsequently, the increase in exposures adds to the cumulative lifetime dose of the population and makes radiation safety an ever-growing concern. Therefore, new dose measurement systems are of fundamental importance.

1.2 CBCT TECHNOLOGY

CBCT technology was first introduced in 1977 (Ganguly 2009) and later adapted for clinical use in 1982 at the Mayo Clinic Biodynamics Research Laboratory (Rochester, MN, USA) (Miracle 2009). Initial interest focused primarily on applications in angiography (Robb 1982) in which soft-tissue resolution could be sacrificed in favor of high temporal and spatial-resolving capabilities (Jaju 2014). Since that time, several CBCT systems have been developed for use both in the interventional suite and for general applications in CT angiography and radiation therapy (Wallace 2008). In 1997, CBCT technology was adapted for maxillofacial purposes (Mozzo 1998), and in 1999 the first CBCT device (NewTom QR DVT 9000; Quantitative Radiology, Verona, Italy) was initially introduced in Europe (Mozzo 1998). The device became commercially available for maxillofacial imaging in 2001. Today, CBCT technology is becoming increasingly popular amongst maxillofacial radiologists and surgeons and has become instrumental in implant dentistry, orthodontics, endodontics, and maxillofacial surgery (Dawood 2009).

During gantry rotation (180° - 360°), the x-ray cone beam covers a cylindrical-shaped field of view (FOV) that incorporates the entire captured volume of data (Dawood 2009). The 2D projection images are acquired during the gantry rotation by either using continuous or pulsed radiation from the x-ray source (Scarfe 2008). The benefits of pulsing are reduced dose and the minimization of gantry movement artifacts in the images. The resulting “frames” are recorded as a multiple 2D projection image set during gantry rotation using a flat panel detector or image intensifier coupled to a charge-coupled device (CCD). The number of planar projections typically ranges from 150 to more than 600 frames (Scarfe 2008). The 3D images commonly needed for diagnostic purposes are reconstructed from 2D images using a back projection reconstruction algorithm first described by Feldkamp et al. (Feldkamp 1984). To date, more sophisticated algorithms commonly use filtered back-projection to generate 3D volumetric data (Scarfe 2007).

The major advantages of CBCT devices (Fig. 1.1), when compared to MSCT devices, are their shorter examination time (Scarfe 2008), high-contrast resolution (Suomalainen 2010), and low effective dose capabilities (Loubele 2009). However, CBCT devices induce scatter radiation that is considerably higher than that of MSCT devices. Further disadvantages of CBCT devices are increased beam hardening artifacts (Draenert 2007) and poor soft tissue contrast (Arai 1999), (Scarfe 2008).

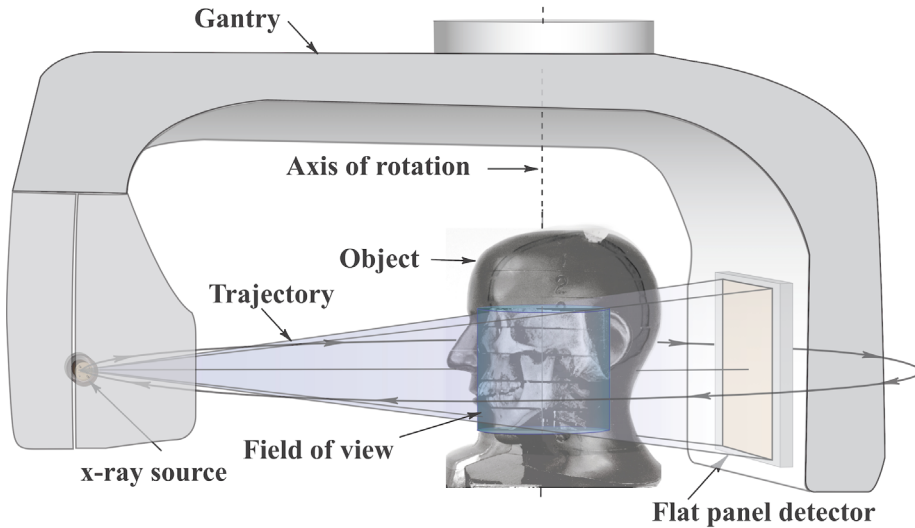


Fig. 1.1. Schematic presentation of CBCT scanning device

1.3 DOSIMETERS AND DOSE ASSESSMENT METHODS

A radiation dosimeter is a device, instrument, or system that measures or evaluates, either directly or indirectly, the quantity of exposure, kerma, absorbed dose or equivalent dose, or their time derivatives (rates), or related quantities of ionizing radiation. A dosimeter along with its reader is referred to as a dosimetric system (Izewska 2005). Dosimeters measure the absorbed dose (D) that is defined as a quantity of radiation energy (Joule) deposited per unit mass (kg) of tissue (Gray = J/kg) (IAEA No. 457, 2007), (ICRU 33).

At present, a number of different dose measurement methods are commonly used. Effective dose assessments can be performed either by using the computed tomography dose index (CTDI) or by using organ point dose measurements in anthropomorphic phantoms. The effective dose is typically calculated from the organ doses using tissue weighting factors recommended by the International Commission on Radiological Protection (ICRP) Publication 103 (ICRP 103).

CTDI: The CTDI has been most commonly applied for dose assessments in multi-slice computed tomography (MSCT) devices (McCollough 2011), (Kim 2011a), (Yu 2009), (Roxby 2009), (Pauwels 2012), (Lofthag-Hansen 2008), (Thilander-Klang 2010). The CTDI was originally developed for fan beam (360°) spiral and helical gantry rotation CT dose assessment (Shope 1981). The major benefit of the CTDI is the standardized measurement method and the ease of use. However, one setback

of the CTDI in CBCT effective dose assessments is the need for dose conversion factors, especially when performing a partial gantry rotation (e.g. 210°) around the patient. Furthermore, the CTDI values are commonly measured using a 100 mm long pencil chamber with the assumption that the collimated x-ray beam and penumbra are contained within the length of the dose meter. This does not apply to CBCT devices, however, where the FOV length is larger than the length of the pencil chamber (Boone 2007), (Mori 2005), (Pauwels 2012).

The effective doses caused by MSCT or CBCT devices are traditionally measured using anthropomorphic phantoms and different dosimeters. At present, the most commonly used dosimeters are thermoluminescent dosimeters (TLD), optically stimulated luminescent dosimeters (OSLD), radio-photoluminescence dosimeters (RPLD), and metal oxide semiconductor field effect transistor dosimeters (MOSFET).

TLD: Traditionally, effective dose assessments in the maxillofacial region have been performed using anthropomorphic phantoms combined with thermoluminescent dosimeters (TLD) (Ludlow 2003), (Kau 2005), (Ludlow 2006), (Ludlow 2008), (Kiljunen 2008), (Roberts 2009), (Suomalainen 2009), (Pauwels 2010), (Qu 2010), (Rottke 2013). A review of TLD dosimeter history is presented by Aschan (Aschan 1999).

The benefit of TLDs is their capability to measure very low doses (Tarr 1998), (Dong 2002) and linear response to photon energies (Dong 2002), (Bower 1998). However, one major drawback when using TLDs is their lack of real-time measurement capabilities. Furthermore, the dosimeters need to be replaced after every exposure (I, IV) making extensive studies more laborious, time consuming, and prone to error and imprecision (III).

OSLD: Optically stimulated luminescent dosimeters have been used for effective dose assessment in tissue equivalent (ATOM) phantoms (Ludlow 2013). The major benefits of OSL dosimeters are their high sensitivity and ease of use. Nevertheless, similarly as in the case of the TLDs, the OSLDs have to be removed from the phantom for dose read-out and erasure procedures.

RPLD: Radio-photoluminescence dosimeters (RPLD) have also been used for therapeutic applications (Akselrod 2006) and effective dose evaluation with anthropomorphic phantoms (Manninen 2014a), (Manninen 2014b).

MOSFET: MOSFET dosimeters have been previously used in diagnostic radiology (Lian 2011), (Lian 2012), patient dosimetry (Briere 2008), and entrance surface dose measurements in diagnostic radiology (Peet 1999). MOSFET dosimeters are manufactured using semiconductor fabrication process and were first described

in 1959 by John Atalla and Dawon Kahng (Kahng 1963). Since then, MOSFET technology has been used in personal dosimetry (O'Connel 1998), (Sarrabayrouse 2004) and medical applications (Price 2004), (Ramaseshan 2004), (Lavallee 2006), (Tarr 2004), (Kohno 2006) (Lee 2011), (Kim 2010a), (Kim 2010b), (Kim 2011b), (Miksys 2010).

The major benefits of MOSFET dosimeters are their real-time measuring capability and the possibility to perform multiple measurements without the need to repeatedly dismantle and reposition the phantom. However, the drawbacks of MOSFET dosimeters are their low sensitivity when compared with TLDs and their limited lifetime due to the accumulated dose. A further limitation of MOSFETs is their variation of angular sensitivity. When comparing MOSFETs to TLDs, it must be taken into consideration that their uncertainty is greater than 25% at doses less than 1.7 mGy. Therefore, MOSFETs are commonly used in radiotherapy where much higher doses are applied (Spezi 2012), (Kouno 2013) (Miracle 2009)

2 AIMS AND STRUCTURE OF THE THESIS

The first aim was to characterize MOSFET dosimeter sensitivity, energy, dose, and angular dependencies to assess their suitability for low-dose CBCT measurements in anthropomorphic phantoms.

A second aim was to validate a newly developed dose measurement setup for effective dose assessment in anthropomorphic phantoms using Monte Carlo simulations and TLD measurements.

The third aim was to apply the newly developed measurement setup to assess the effective doses resulting from three CBCT and one MSCT device.

The thesis is based on five original articles referred to in the text by their Roman numerals.

ARTICLE I:

Koivisto J, Wolff J, Kiljunen T, Schulze D, Kortensniemi M. “*Characterization of MOSFET dosimeters for low-dose measurements in maxillofacial anthropomorphic phantoms*” **J Appl Clin Med Phys.** 2015 Jul 8;16(4):5433.

In this study, 20 MOSFET dosimeters were characterized for two CBCT photon energy ranges (34.2–50.8 keV, 41.2–61.1 keV), dose properties, and organ dose measurements using TLD dosimeters as a reference. In addition, MOSFET dosimeter uncertainty was assessed by repetitive measurements at different doses.

ARTICLE II:

Koivisto J, Kiljunen T, Wolff J, Kortensniemi M. Characterization of MOSFET dosimeter angular dependence free-in-air and in soft tissue equivalent material for three-axes rotation. **Journal of Radiation Research**, 2013, 00, 1–7 doi: **10.1093/jrr/rrt015**

In the second article, the MOSFET angular sensitivity was investigated using dental photon energies and soft tissue equivalent backscatter material.

ARTICLE III:

Koivisto J, Kiljunen T, Tapiovaara M, Wolff J, Kortnesniemi M. Assessment of radiation exposure in dental cone-beam computerized tomography with the use of metal-oxide semiconductor field-effect transistor (MOSFET) dosimeters and Monte Carlo simulations.

Oral Surg Oral Med Oral Pathol Oral Radiol. 2012 Sep;114(3):393-400.

In the third study, a dose measurement setup was developed. The setup comprised 20 MOSFET dosimeters that were placed into allocated grid holes of an anthropomorphic RANDO phantom. The MOSFET dose measurement setup was validated using Monte Carlo simulations.

ARTICLE IV:

Koivisto J, Schulze D, Wolff J, Rottke D. Effective dose assessment in the maxillofacial region using thermoluminescent (TLD) and metal-oxide semiconductor field-effect transistor (MOSFET) dosimeters; A comparative study.

Dentomaxillofacial Radiology. 2014 43(8)

In the fourth study, the previously developed MOSFET dose measurement setup was validated using TLD dosimeters (IV) that were placed in an anthropomorphic head phantom. The dose measurements were performed using four typical CBCT head examination protocols.

ARTICLE V:

Koivisto J, Järnstedt J, Dastidar P, Wolff J, Kortnesniemi M. The effect of supine, prone and oblique head positioning on the effective dose in Cone Beam CT technology.

Oral Surg Oral Med Oral Pathol Oral Radiol. 2014 Sep;118(3):355-62. doi: 10.1016/j.oooo.2014.05.016. Epub 2014 Jun 14.

In the fifth article, the MOSFET dose measurement setup was used for organ and effective dose assessment resulting from supine, prone, and oblique phantom positions in three CBCT and one MSCT device.

3 MATERIALS AND METHODS

3.1. DOSIMETERS

3.1.1 MOSFET DOSIMETERS

MOSFET dosimeters (TN-1002RD-H) comprise an n-type semiconductor substrate that is isolated from the metal gate (G) by a very thin silicon oxide (SiO_2) layer (Fig. 3.1.1A). Ionizing radiation causes the generation of electron-hole pairs in the SiO_2 layer. Some of the holes near the Si- SiO_2 interface become trapped causing a stable, negative shift (DV_{TH}) for a predetermined drain (D) – source (S) current (I_{DS}) that is proportional to the radiation dose. Several investigators have reported the operating principles of the MOSFET dosimeter (Tarr 1998), (Soubra 1994), (Sarrabayrouse 1994). The TN-1002RD-H dosimeter used in this study comprised two MOSFETs with an active area of 0.04 mm^3 that were fabricated on a silicon rectangle (a die) mounted on a flexible polyamide (PCB) cable and encapsulated with black 1.02 mm thick (II) epoxy resin (Fig. 3.1.1B) (G1 and G2 are metal gates (G), D1 and D2 are drains (D)).

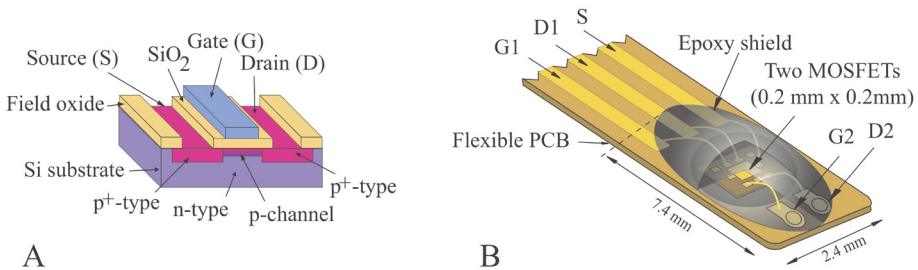


Fig. 3.1.1. MOSFET dosimeter structure (A) and TN-1002RD-H dosimeter (B)

All absorbed doses were measured using a mobile MOSFET device TN-RD-70-W20 (Best Medical Canada, Ottawa, Canada). The TN-RD-70-W20 MOSFET device comprises a TN-RD-38 wireless Bluetooth transceiver, four TN-RD-16 reader modules, twenty high-sensitivity TN-1002RD-H dosimeters, and TN-RD-75M software. In this thesis, the TN-RD-16 reader modules were operated using the high bias voltage (13.6 V) to obtain the highest (mV/mGy) sensitivity. A TN-RD-38 Bluetooth transceiver was used for data communication between the TN-RD-16

reader modules and a PC. Four TN-RD-16 reader modules and their power supplies are shown in Fig. 3.1.2.



Fig. 3.1.2. Four MOSFET TN-RD-16 reader modules

3.1.2. REFERENCE DOSIMETERS

Prior to their use, all MOSFET dosimeters were characterized for their performance by comparing their results with those obtained using a calibrated ionization chamber dosimeter and a multi-purpose dosimeter. The dose area product (DAP) value required for the Monte Carlo simulation program (PCXMC) was measured using a ionization chamber dose area product (DAP) dosimeter. Furthermore, TLD dosimeters were used for comparative dose point dose measurements in the head phantom and in the MOSFET validation process.

Ionization chamber dosimeter: MOSFET dosimeter energy, dose, dose rate, and accumulated dose dependency reference readings were attained using a RADCAL 1015 dosimeter and a RADCAL 10X5-6 ionization chamber (IC) (Radcal Corporation, Monrovia, CA, USA). The sensitivity variation of the ionization chamber was less than $\pm 1\%$ in the 30–70 keV range.

Multi-purpose detector: The MOSFET dosimeter uncertainty was evaluated using a Barracuda multi-purpose detector (MPD) (RTI Electronics AB, Mölndal, Sweden). The MPD is capable of measuring ranges between 0.1 μGy –1000 Gy and has less than $\pm 1\%$ energy sensitivity variation between 50–90 kVp.

Ionization chamber DAP-meter: The dose area product (DAP) values were measured using a KermaX-plus IDP 120–104 Hs meter (IBA Dosimetry GmbH, Germany). Prior to the MOSFET characterization measurements, the multi-purpose detector, the ionization chamber dosimeter, and the ionization chamber DAP dosimeter were

calibrated at the secondary standard dosimetry laboratory (SSDL) of the Finnish Radiation and Nuclear Safety Authority (STUK) that is traceable to primary standard dosimetry laboratory (PSDL).

TLD 100: TLD dosimeters (TLD 100; Thermo Fisher Scientific, Waltham, MA) were used to compare their performance with MOSFETs in an anthropomorphic RANDO phantom. TLD dosimeters emit light that is proportional to the radiation dose when heated after the irradiation exposure (IAEA No. 457, 2007). The reset and annealing procedures of the TLDs were made in a microprocessor-controlled TLD oven (PTW, Freiburg, Germany). The TLD read-out sequence was performed in a Fimel LTMWin (Fimel, Fontenay-aux-Roses, France) device. TLD calibration and read-out procedures were performed according to a method previously described by Rottke et al. (Rottke 2013) with traceability to secondary standard dosimetry laboratory (SSDL, Freiburg, Germany).

3.2. CHARACTERIZATION OF MOSFET DOSIMETERS

MOSFET dosimeter characterization was performed to evaluate their feasibility for low-dose measurements in an anthropomorphic phantom using dental photon energies. The characterization procedure consisted of energy, dose, dose rate, accumulated dose, and angular dependency measurements. In addition, the MOSFET dosimeter combined uncertainties were assessed.

3.2.1. PHOTON ENERGY DEPENDENCY

Defining the energy dependency characteristics of a dosimetric system (Izewska 2005) is important when dosimeters are used with different mean photon energy spectra. Furthermore, when MOSFETs are used for organ dose measurements their energy response should be known because the mean photon energy is affected by the attenuation of different tissues. Ideally, MOSFET dosimeters should be characterized according to the radiation qualities close to those for which the dose measurements are needed (Buerman 2010).

In previous studies by Peet et al., Dong et al., and Manninen et al. (Peet 1999), (Dong 2002), (Manninen 2014a), the MOSFET energy dependency was evaluated as a function of tube voltage. This method, however, does not take into account the energy spectra or the mean photon energy of the x-ray device that is affected by the tube voltage and filtration used. In this study, however, the MOSFET energy sensitivity was evaluated as a function of the mean photon energy (keV) using two

different filter combinations and a range of tube voltages. This method was chosen to encompass the typical mean photon energies used in dental and maxillofacial diagnostic procedures.

In this thesis, the photon energy sensitivity measurements were performed using 20 MOSFET dosimeters that were attached to an in-house constructed carbon fiber frame. The MOSFET positions were carefully chosen as a linear array perpendicular to anode-cathode direction to minimize the heel effect in the anode-cathode direction. The subgroups of ten dosimeters on both sides of the (RADCAL) 10 x 5-6 ionization chamber (Fig. 3.2.1) were interchanged to compensate for possible variations in dose across the field. The measurements were repeated 10 times and an average calibration coefficient (mV/mGy) was calculated. In order to include the backscatter radiation, a (15 cm x 15 cm x 10 cm thick) PMMA block was attached to a carbon fiber holder to simulate soft tissue interactions (IAEA No. 457, 2007). The PMMA block dimensions were chosen based on a study by Khan et al. (Khan 2003) and were considered, therefore, to provide sufficient backscatter for the Cu HVLs (mm) used in this study (Table 1).

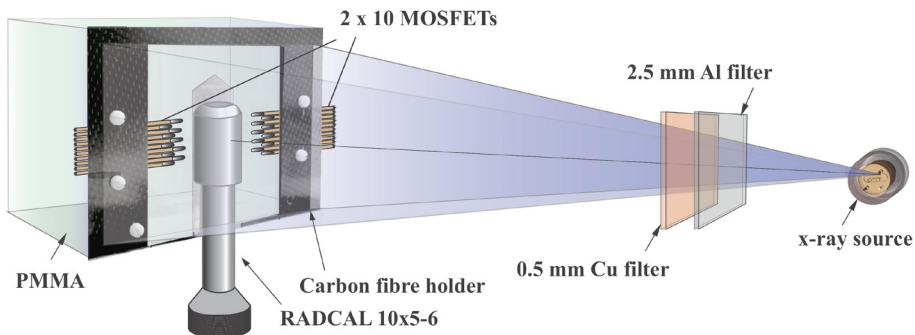


Fig. 3.2.1. MOSFET dosimeter energy dependency measurement set-up

The energy dependency measurements were carried out using a Promax 3D CBCT device operated without gantry rotation and constant doses to minimize possible dose or angular dependency (Al 2.5 mm filter: 17.6 ± 0.2 mGy, Al 2.5 mm + 0.5 Cu: 20.6 ± 0.4 mGy). The tube voltage range was 50 – 90 kVp with 5 kVp increments. The differences in the doses were caused by the different mAs values in the experimental setup.

In this thesis, mean photon energies and HVLs were calculated using a computer program (Tapiovaara 2008a) that is based on the semi-empirical spectrum model described by Birch and Marshall (Birch 1979). The mean photon energies, HVLs and tube voltages (kVp) used are presented in Table 1.

Table 1. The calculated mean photon energies and corresponding Cu HVL's using 2.5 mm Al and 2.5 mm AL+0.5 mm Cu filter combinations

Tube Voltage kV	Al (2.5mm)			Al (2.5 mm) +Cu (0.5 mm)		
	Mean E keV	HVL		Mean E keV	HVL	
		Cu (mm)	Al (mm)		Cu (mm)	Al (mm)
50	34.2	0.072	2.26	41.2	0.161	4.50
55	36.4	0.081	2.54	44.2	0.192	5.11
60	38.6	0.093	2.80	46.9	0.224	5.68
65	40.7	0.104	3.06	49.6	0.258	6.22
70	42.8	0.115	3.33	52.2	0.294	6.73
75	45.0	0.129	3.61	54.7	0.333	7.24
80	47.1	0.144	3.91	57.1	0.373	7.71
85	49.0	0.159	4.21	59.2	0.411	8.12
90	50.8	0.176	4.50	61.1	0.448	8.49

The MOSFET calibration coefficient (CC) was calculated using the MOSFET read-out value (mV) that was subsequently divided by the dose (mGy) and simultaneously measured using an ionization chamber dosimeter (Brady 2012). Each MOSFET calibration coefficient was calculated separately and since the sensitivity differences between the dosimeters were minimal, thus the average sensitivity result was reported.

3.2.2. DOSE, DOSE RATE, AND ACCUMULATED DOSE DEPENDENCIES

Ideally, a dosimeter reading should be linearly proportional to the dosimetric quantity and be independent of the radiation dose rate used for the measurements (Izewska 2005). Furthermore, dosimeters should always be characterized for their sensitivity since their lifetime dose history affects their sensitivity.

In order to obtain dose, dose rate, and accumulated dose dependencies, 20 MOSFET dosimeters were irradiated 10 times on the Promax 3D CBCT device (Planmeca Oy, Helsinki, Finland). All exposures were performed using 80 kVp with a 2.5 mm Al filter and 47.1 keV mean photon energy. To attain MOSFET dose dependency, the irradiation was performed using seven different mAs values (10, 20, 40, 80, 160, 320, and 640 mAs) over a dose range from 0.24 to 17.5 mGy. The average dosimeter responses were calculated for each dosimeter and dose value. The dose rate dependency was evaluated using a constant dose of 16.4 mGy with five different dose rates (0.16, 0.32, 0.67, 1.34, and 2.70 mGy/s). The mean dose rate dependency was calculated for each dosimeter and dose rate. In order to assess the MOSFET dosimeter accumulated dose sensitivity, an energy dependency setup

was used (Fig. 3.2.1). The sensitivities of the 20 MOSFET dosimeters were measured after dismantling the dosimeters from the phantom at a 17,500 mV accumulated threshold voltage. The MOSFET sensitivity was calculated based on the two different threshold voltages: 8,300 mV (after the calibration procedure) and 17,500 mV (after dismantling the dosimeters from the phantom).

3.2.3. ANGULAR DEPENDENCY

The dosimeter response variation with the angle of incidence of radiation is known as the directional or angular dependency (Izewska 2005). When performing dose measurements on CBCT devices, it is necessary to take the angular sensitivity dependency of the dosimeters into account because the MOSFET dose response varies depending on the angle of incidence. The major cause of this phenomenon is the asymmetrical geometry of the dosimeter.

In this thesis, the angular dependency measurements were performed using a soft tissue equivalent PMMA phantom. All x-rays used for defining the angular dependencies were generated using a Promax 3D cone beam CT x-ray device using 80 kV tube potential (HVL 7.7 mm Al), 100 mAs tube current exposure time product, and 2.5 mm Al + 0.5 mm Cu filtration.

The mean and standard deviation (1SD) of the reference air kerma measured in a single exposure (one of the five repeated exposures in each angular step) with an ionization chamber was 6.9 ± 0.2 mGy. All CBCT exposures were performed using an operating mode that disables the gantry rotation of the CBCT device, and thereby offers a fixed and stationary x-ray source. MOSFET dosimeter sensitivities were normalized to a 0-degree reading of the corresponding axis of rotation. The definition for zero degree orientation of the dosimeter is shown in Fig. 3.2.2 for each axis of rotation.

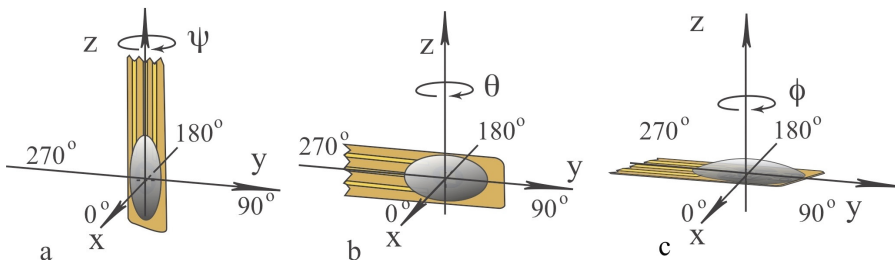


Fig. 3.2.2. Irradiation geometry description for the angular sensitivity dependency measurements of the MOSFET dosimeter with axial (a), normal-to-axial (b), and tangent-to-axial rotation (c) co-ordinate axes and rotation angles

The angular dependency coefficients (C_ψ , C_θ , C_ϕ) were determined as follows (II):

$$C_\psi = \frac{D(\psi)}{\bar{D}(\psi)}, C_\theta = \frac{D(\theta)}{\bar{D}(\theta)}, C_\phi = \frac{D(\phi)}{\bar{D}(\phi)} \quad (1)$$

where $D(\psi)$, $D(\theta)$, and $D(\phi)$ are the average doses from five repeated exposures at rotation angles ψ , θ and ϕ , and $\bar{D}(\psi)$, $\bar{D}(\theta)$ and $\bar{D}(\phi)$ are the average doses over all angle orientations for each rotation axis, respectively. Each angular position was measured with five repeated exposures to verify reproducibility and improve reliability and to determine the standard deviation (1SD) for that angular position. Specifically, the relative standard deviation (1SD) was determined for each rotation axis and within each angular position, relative to the angle specific mean value. The comparative MOSFET mean sensitivities between the studied rotational axes were verified with separate measurements in continuous full rotation exposures using three MOSFET detectors that were interchanged between repeated exposures to exclude individual detector sensitivity variations.

Measurements: The angular dependency measurements were performed using a fixed x-ray source and a rotating in-house constructed cylindrical acrylic phantom that was 80 mm in diameter. Dose measurements were performed in three-axes using three dosimeters placed in 2.5 mm holes. (Fig. 3.2.3.) The smallest possible (2.5 mm) drill hole size was chosen to minimize the air gap and the “hole effect” caused by non-attenuated direct radiation. The in-house constructed PMMA phantom was rotated 360 degrees with five-degree increments (i.e. 72 measured directions per rotation) using a mechanical support resting on ball bearings. A reference reading of every exposure was simultaneously attained using a RADCAL 1015 dosimeter and a RADCAL 10X5-6 ionization chamber (Radcal Corporation, Monrovia, CA, USA). A separate dial ring for adjusting the rotation angle was attached to the lower part of the phantom (Fig. 3.2.3.). The alignment of the phantom was assessed with $\pm 1^\circ$ accuracy using three laser lines generated by the CBCT x-ray device. The PMMA phantom included a hole for the ionization chamber. The ionization chamber was fitted tightly into the hole to avoid any air-gap between the PMMA and the dosimeter. The ionization chamber remained stationary during the measurements while the PMMA cylinder and MOSFET dosimeters were rotated around the axis that was perpendicular to the anode-cathode axis to eliminate variations in irradiation caused by the heel effect (Fig. 3.2.3.).

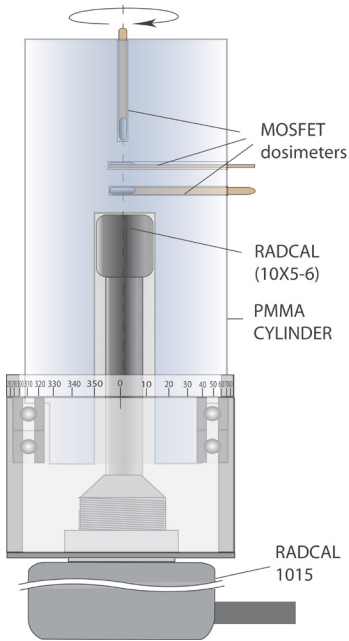


Fig. 3.2.3. The rotation mechanism, MOSFET dosimeters, ionization chamber (RADCAL 10X5-6), and PMMA backscatter material

3.2.4. MOSFET DOSIMETER UNCERTAINTY

Uncertainty is an interval about the average value of a series of measurements or calculations that, within a certain level of confidence, is believed to contain the “true” value of quantity (Mitch 2009). In this thesis, the MOSFET dosimeter uncertainty was assessed according to the UK National Dose protocol (NRPB, 1992), where the maximum patient dose uncertainty has been proposed to be 25% at 95% confidence interval (CI). In order to evaluate the uncertainty, all MOSFET and multi-purpose dosimeters (MPD) were simultaneously exposed to 80 kVp (47.1 keV, HVL 7.71 mm Al, SID 600 mm) using a Promax 3D CBCT device (Planmeca Oy, Helsinki, Finland) with a 2.5 mm Al filter. The x-ray source was operated without gantry rotation using seven mAs values (10, 20, 40, 80, 160, 320, and 640 mAs). The corresponding doses were as follows: 0.24, 0.52, 1.1, 2.2 4.4, 8.8, and 17.6 mGy, respectively.

The MPD dosimeter calibration coefficient (1.018) for 80 kVp tube voltage (2.5 mm Al + 0.5 mm Cu) was used to convert the dosimeter reading to the true dose. The calculated expanded uncertainty (2SD) of the MPD using 10 averaged samples was 1.1%. The combined uncertainty (u_c) was calculated as a quadratic summation of the uncertainties of MPD and MOSFET readout uncertainties ($k=2$). Furthermore,

the lowest acceptable dose using one exposure and the required number of samples to attain low dose limit (0.3 mGy) were assessed.

The combined uncertainties (u_c) of the photon energy sensitivity measurements were assessed as a weighted sum of variances. These included the ionization chamber expanded (2SD) energy sensitivity uncertainty 2% (30–70 keV) obtained from the RADCAL 1015 datasheet, MOSFET dosimeter calibration factor variation as a function of saturation voltage (4%) (I) (Koivisto 2014), and the estimated position uncertainty (2%) and cable irradiation uncertainties (1%) according Ehringfeld et al. (Ehringfeld 2005).

3.3. HEAD PHANTOM USED FOR EFFECTIVE DOSE ASSESSMENT

In order to define the effective doses in the maxillofacial region, an anthropomorphic radiation analogue dosimeter (RANDO) phantom was used. All measurements in this thesis were performed using a RANDO RAN102 male head phantom (Radiation Analogue Dosimetry System; The Phantom Laboratory, Greenwich, NY, USA). The phantom comprised a human skull cast in a soft-tissue-equivalent material to match the attenuation and scattering conditions of the bone, soft tissues, and airways of the human head. The phantom was composed of ten 25 mm thick layers numbered in order from 0 to 9 from the calvaria to the neck area (Fig. 3.3.1.). Each layer had a grid of holes (\varnothing 5 mm) filled with detachable soft-tissue equivalent plugs for dosimeter placement.

In order to measure the absorbed doses of the most radiosensitive organs, twenty MOSFET and 40 TLD dosimeters were positioned into different layers of the RANDO head phantom. The twenty MOSFET dosimeters were positioned into the phantom head layers (Fig. 3.3.1.) according to a protocol described by Ludlow et al. (Ludlow 2006). However, in this study, the dosimeters in the calvarium posterior, calvarium left, left lens, and left orbit were not included. The reason that only 20 dosimeters were used in the present study was based on the assumption that the organ dose in the brain area is relatively low and that the dose in the left eye and the left orbit would be the same as that of the right side in symmetric imaging geometry (III).

All dosimeters were placed in allocated grid holes with their epoxy bulbs facing in the anterior direction in order to assess the gantry rotation sensitivity variations of the scans. In addition, the MOSFET cables were routed from the phantom skull base through the prefabricated airway compartments and the unused dosimeters voids to the designated layers. The phantom layers were then stacked on top of each other to avoid any gaps between them. The placement of the dosimeters with the corresponding layers in the phantom is presented in Fig. 3.3.1.

Phantom Location	Phantom Dosimeter		Phantom level
	Level	number	
Calvarium anterior	2	1	
Mid brain	3	2	
Pituitary fossa	3	3	
Right orbit	4	4	1
Right lens	4	5	2
Right cheek	5	6	
Right ramus	6	7	3
Left ramus	6	8	4
Right parotid	6	9	5
Left parotid	6	10	
Center C-spine	7	11	
Left back neck	8	12	
Right mandible body	7	13	6
Left mandible body	7	14	
Right submandibular gland	8	15	7
Left submandibular gland	8	16	
Center sublingual gland	8	17	
Midline thyroid	9	18	8
Thyroid surface	9	19	
Pharyngeal-esophageal space	9	20	9

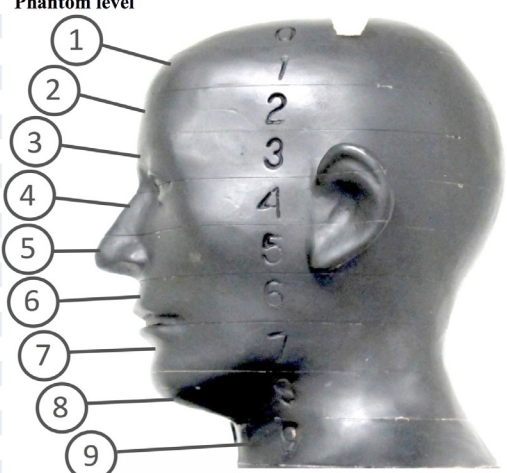


Fig. 3.3.1. MOSFET dosimeter placement in RANDO phantom

3.4 EQUIVALENT AND EFFECTIVE DOSE ASSESSMENT

Equivalent dose (H_T) and effective dose (E) are defined as radiation protection quantities (Suomalainen 2010). Equivalent dose is a quantity that is used for the comparison of different radiation types. Equivalent dose is calculated based on the absorbed dose and furthermore takes the biological effectiveness of the radiation into account. Effective dose quantity allows a comparison of the stochastic risks induced by different imaging protocols, i.e. x-ray sources. Effective dose (Sievert, (Sv)) is calculated according to the recommendations set by the International Commission on Radiological Protection (ICRP). Effective dose calculation is performed by multiplying the organ doses by their weighting factors based on the radiation sensitivity of each organ.

In this thesis, the equivalent dose or radiation-weighted dose H_T for all organs or tissues T was calculated using the following equation (Pauwels 2010), (Loubele 2009) (III), (IV), (V):

$$H_T = w_R \sum_i f_i \cdot D_{Ti} \quad (2)$$

where the radiation weighing factor $w_R = 1$ (Sv/Gy) for x-rays, f_i the mass fraction of tissue T in layer i, and D_{Ti} being the average absorbed dose of tissue T in layer i. Summation is done for all phantom layers between 0 and 9. The dosimeter locations chosen in this study represent the most radiosensitive organs in the maxillofacial and neck area. The fraction in the head and neck area ($\Sigma(f_i)$) of most organs including the thyroid gland, brain, salivary glands, extrathoracic airways, and oral mucosa is 1. This is because these organs are located within the RANDO phantom layers. It has been estimated that the proportion of lymphatic nodes and muscle in the head and neck area represent 5% of the total body mass. According to Ludlow et al. (Ludlow 2003), the fraction of irradiation in the esophagus is 10% and the skin surface area in the head and neck area is 5% of the total body skin area.

The effective dose was obtained from measured organ doses using the revised guidelines given by the International Commission on Radiological Protection (ICRP 103, 2008). The effective dose E is calculated by the following equation (III), (IV), (V):

$$E = \sum_T w_T \cdot H_T, \quad (3)$$

where w_T is the weighting factor of tissue T and H_T is the equivalent dose in tissue T. According to the ICRP recommendation, the calculation of effective dose is based on a large number of organs and tissues in the body and the sum of their weighting factors w_T is 1. Some of the organs considered in the calculation are grouped as “remainder tissues”. The w_T for the remainder tissues specified by ICRP 103 is 0.12.

The equivalent dose in bone marrow and the bone surface was calculated by averaging the equivalent doses of the corresponding dosimeters representing the organ. Finally, the contribution to the effective dose was calculated using specific fractions irradiated and weighting factors. The ICRP 103 weighting factors w_T and the fraction of irradiation used in the calculations are shown in Table 2.

Since bone has a higher mass energy absorption coefficient than soft tissue, the bone surface dose was obtained by multiplying the bone marrow dose with the mass energy absorption coefficient ratio of bone and soft tissue at the average photon energy. In this thesis, the average energy was calculated using a computer program (Tapiovaara 2008a) that is based on the semi-empirical spectrum model described by Birch and Marshall (Birch 1979). The calculated average energy of the spectrum is 58.8 keV, and the ratio of the mass energy absorption ratios of bone and soft tissue (NBS Handbook No. 85 1964) is 3.23. This value was used to multiply the bone marrow doses to obtain the bone surface doses.

Table 2 ICRP 103 tissue weighting factors (w_T), fractions irradiated (f_i), and the dosimeters used to calculate the effective dose (III).

Tissue	w_T	f_i	Dosimeter number
Thyroid	0.04	1	18, 19
Esophagus	0.04	0.1	20
Brain	0.01	1	2, 3
Skin	0.01	0.05	5, 6, 12
Salivary glands	0.01	1	
Parotid			9, 10
Submandibular			15, 16
Sublingual			17
Bone marrow	0.12	0.165	
Mandible		0.013	7, 8, 13, 14
Calvaria		0.118	1, 4
Cervical spine		0.034	15
Bone surface*	0.01	0.165	
Mandible		0.013	7, 8, 13, 14
Calvaria		0.118	1, 4
Cervical spine		0.034	15
Remainder	0.12		
Lymphatic nodes		0.05	9, 10, 15-17
Extrathoracic airway		1	4, 11, 18, 20
Muscle		0.05	9, 10, 15-17
Oral mucosa		1	7-10, 13-17

*Bone surface dose = bone marrow dose x 3.23.

3.5. MOSFET SETUP USED FOR EFFECTIVE DOSE ASSESSMENT

The effective dose assessment setup consisted of an anthropomorphic RANDO phantom, MOSFET dosimeters, MOSFET dosimeter readers, and corresponding power supplies. All MOSFET dosimeters were placed into allocated organ positions in the phantom. The RANDO phantom head was attached to a carbon fiber mechanism supported by a camera holder to allow the phantom to be tilted in different directions (Fig. 3.5.1).



Fig. 3.5.1 The MOSFET measurement setup with four TN-RD-16 reader modules, RANDO phantom, and a ProMax 3D MID CBCT device (I).

3.6. VALIDATION OF THE MOSFET DOSE MEASUREMENT METHOD

In the validation process, the MOSFET measurement setup was evaluated for its suitability for effective dose assessments using typical dental exposures. Validation was performed using two different methods that were based on simulations and comparative dose measurements using TLD dosimeters in identical conditions.

3.6.1. EFFECTIVE DOSES DETERMINED USING MOSFETS AND MONTE CARLO SIMULATIONS

PCXMC (Radiation and Nuclear Safety Authority, Helsinki, Finland) (Tapiovaara 2008b) is a widely used Monte Carlo-based simulation program for calculating absorbed organ doses and effective doses in x-ray examinations based on measurable quantities, e.g. dose area product (DAP) or incident air kerma (ICRU 74, 2005). Monte Carlo calculations are based on the stochastic mathematical simulation of interactions between photons and matter. Photons are emitted (in a fictitious mathematical sense) from a point source into the solid angle specified by the focal distance and the x-ray field dimensions. The photons are then followed while they randomly interact with the phantom according to the probability distributions of the physical processes that they may undergo: photo-electric absorption, coherent (Rayleigh) scattering or incoherent (Compton) scattering (Tapiovaara 2008b). In PCXMC, organ doses and the effective dose are calculated using a modified anatomical phantom based on a mathematical hermaphrodite phantom model described by Cristy and Eckerman (Cristy 1987). When calculating the effective dose,

the tissue weighting factors of both the International Commission on Radiological Protection (ICRP) Publication 103 (ICRP 103,2008) and Publication 60 (ICRP 60, 1990) are used. The latest PCXMC software version (2.0) allows multiple projection simulations in batch mode and has been used for non-dental CBCT examinations (Vassileva 2010), (Podnieks 2012), (He 2010).

MOSFET dose measurements: In order to evaluate the variations in effective dose caused by phantom movement, the organ doses were measured by directing the cone beam to 39 different vertical positions using 0.5 cm increments. The measurements covered layers 2 – 8 (from the calvaria to the thyroid gland) on the RANDO phantom (Fig. 3.6.1). The exposed phantom layers correspond roughly to Z_{ref} values of 76 – 97.5 cm on the MC simulations (Fig. 3.6.2). Ten exposures were performed for each position using 8 x 8 cm field of view (FOV) and standard clinical scan parameters (84 kV, 12 mA, 145 mAs). The absorbed organ doses of ten measurements were averaged and used to calculate effective doses for each vertical position, respectively.

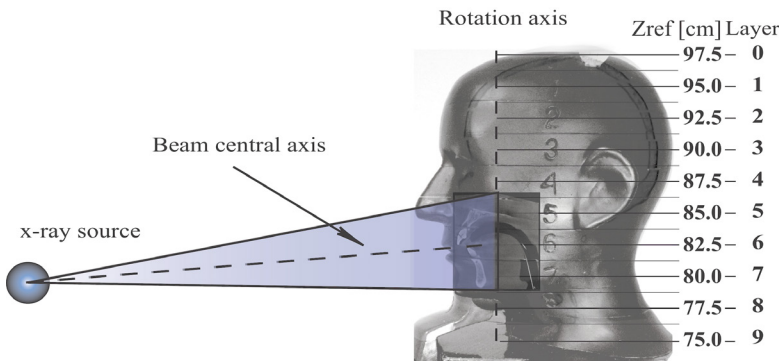


Figure 3.6.1. RANDO phantom head with superimposed PCXMC coordinates (Z) and a variable x-ray beam centerline

Monte Carlo simulations: PCXMC is a Monte Carlo simulation program used to calculate the organ doses of patients in x-ray examinations. The program calculates the organ doses in 29 organs and the effective dose using weighting factors according to ICRP publication 103 (ICRP 103, 2008). In the PCXMC simulation program, the coordinate system has its location of origin in the middle of the base of the trunk of the phantom. The positive Z-axis points upwards, the x-axis to the left hand side, and the y-axis to the back of the phantom. The angles of incidence and a reference point (X_{ref} , Y_{ref} , Z_{ref}) specify the x-ray beam centerline through which the central axis of the x-ray beam is directed. The simulations in this thesis were made for the PCXMC model beam centerline Z_{ref} coordinates between 71 cm and 93 cm. The rotation axis of the simulations was set to Y_{ref} of -5 cm to cover the oral cavity volume. The organ doses and effective doses based on the simulations are

later presented as a function of the x-ray beam height position coordinate Z_{ref} . The head and neck area of the PCXMC phantom with some organs, the focal point, and z- coordinates (cm) are presented in Fig. 3.6.2.

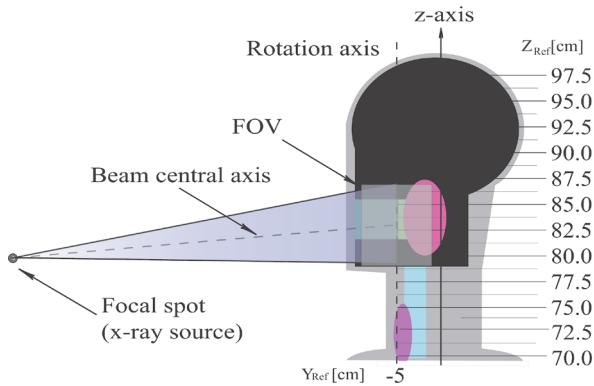


Figure 3.6.2. The PCXMC phantom model showing the neck and head area, the focal point and z- coordinates

Effective and absorbed dose simulations were performed using an 8 x 8 cm field of view (FOV). The dose normalization was based on the measured DAP values from the CBCT exposures. The DAP values were measured ten times using standard clinical scan parameters (84 kV, 12 mA, 145 mAs) and a KermaX-plus IDP 120–104 Hs meter (IBA Dosimetry GmbH, Germany). The average DAP value was 574 mGy \cdot cm 2 . The simulations were made based on the uniform angular output of the CBCT system and covering a rotation angle range of 200 degrees with two-degree graduation in 101 steps: the DAP value for each individual projection of the simulation was 5.68 mGy \cdot cm 2 . The simulations included organ doses for all tissues and organs specified by the ICRP dosimetry formalism such as active bone marrow, thyroid gland, esophagus, skin, salivary glands, and brain.

3.6.2. MOSFET AND TLD COMPARISONS

The feasibility of the MOSFET dosimeters in effective dose assessment was validated by comparing their performance with those of TLD dosimeters in an anthropomorphic head phantom using four different CBCT head examination protocols (Table 3.). Consecutive measurements were performed using 40 TLD and 20 MOSFET dosimeters that were alternately placed in 20 designated sites in the RANDO phantom (Figure 3.3.1.). The chosen locations represented the most radiosensitive organs in the maxillofacial region. All TLD and MOSFET measurements were repeated 10 times to improve the overall statistical outcome.

Table 3. Exposure parameters of measured protocols (IV)

Protocol name	Face Maxillofacial	Teeth Upper jaw	Tooth Mandible	Teeth Both jaws
	Low dose	Low dose	Low dose	Std. Dose
Protocol no.	1	2	3	4
Tube voltage (kVp)	90	90	90	90
Tube current (mA)	6	4	4	10
Exposure time (s)	18	2.8	2.5	12
Q (mAs)	108	11.4	15.1	121
Voxel edge length (mm)	0.6 x 0.6	0.4 x 0.4	0.4 x 0.4	0.2 x 0.2
Frame number	300	300	300	300
Scan FOV (cm)	20 x 17	8.5 x 5	4 x 5	10 x 10

In order to ensure the reproducibility of the phantom position and to minimize phantom shift or rotation (Ludlow 2009), the RANDO phantom holder was tightly fixed to the CBCT chin support. The acquisition FOVs were controlled using a scout image acquired prior to the actual CBCT exposures. The investigated FOVs are presented in Fig. 3.6.3.

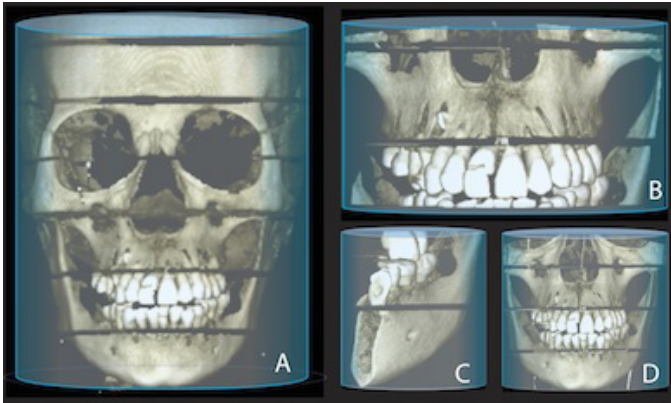


Fig. 3.6.3. Image demonstrating the default CBCT (Promax 3D MID) FOVs used in the study (A) Face (20 x 17), (B) Teeth Upper Jaw (8.5 x 5), (C) Tooth Mandible (4 x 5), (D) Teeth Both Jaws (10 x 10)

In order to obtain absorbed organ doses (mGy), the MOSFET dosimeter readings (mV) were multiplied with the corresponding calibration coefficients (mGy/mV) using the TN-RD-75M software. The comparative effective doses were assessed using two TLD dosimeters at each of the 20 designated sites. The TLD read-out was subsequently multiplied with the calibration factor, averaged, and subtracted by the background radiation according to a previous study by Rottke et al. (Rottke 2013). The effective doses were obtained from the measured organ doses using the revised guidelines given by the ICRP publication 103 (ICRP 103, 2008).

3.7. MOSFET DOSE MEASUREMENT SETUP APPLICATION

In this thesis, the MOSFET setup was used for organ and effective dose assessments resulting from supine, prone, and oblique phantom positions in the maxillofacial region using a novel cone beam computed tomography (CBCT) device and from two conventional dental CBCTs and one multi-slice computed tomography (MSCT) device.

In order to investigate the impact of the CBCT partial (210°) gantry scan on the effective dose in the maxillofacial region, the exposures were performed using a Planned Verity CBCT device (Planmed Oy, Helsinki, Finland) that allowed imaging in supine, prone, and oblique phantom positions (V).

The effective dose attained in different phantom positions and the results acquired using two dental CBCT scanners and an MSCT device using standard protocols were compared. Furthermore, effective dose reference values were obtained using a Promax 3D MAX (Planmeca Oy, Helsinki, Finland), an i-CAT Next Generation (Imaging Sciences International, Hatfield, PA, USA), and a Philips Brilliance-64, (64 slice) (Philips Medical Systems, Eindhoven, Netherlands). The Promax 3D MAX was operated using equivalent exposure parameters (kV, mAs) in a high-resolution mode (face 13 cm), the i-CAT Next Generation was operated in a high-resolution mode (landscape 13 cm), and the MSCT scanner was operated using the manufacturer-recommended, high-resolution imaging protocol. The exposure parameters used for the measurements are presented in Table 4.

Table 4. Exposure parameters used on the MSCT and CBCT scanners (V)

	Planmed Verity CBCT	Promax 3D MAX CBCT	i-Cat Next Gen. CBCT	Philips Brilliance 64 MSCT
Tube voltage (kVp)	96	96	120	120
Tube curr. (mA)	9.5	5	5	93
Exp. Time (s)	6	12	7.4	0.912
Q (mAs)	57	60	37.1	85
Slice thickness (mm)	0.2	0.2	0.25	0.67
Slice increment (mm)	0.2	0.2	0.25	0.33
Pitch (mm)	na	na	na	0.55
CTDIvol (mGy)	na	na	na	11
Voxel (mm)	0.2 x 0.2 x 0.2	0.2 x 0.2 x 0.2	0.25 x 0.25 x 0.25	0.33x0.352x0.352
Scan angle	210°	210°	360°	360°
Pulsed	yes	yes	yes	-
Frame number	300	300	300	-
Scan FOV (cm)	13x16	13x13	13x16	16x18

Phantom positions

Three default patient positions (supine, prone, and oblique) were investigated using a phantom and a Planmed Verity CBCT scanner. In the supine imaging position, the gantry, including the x-ray source and detector, rotates at a 210° angle from the anterior side. In the prone imaging position, the detector rotates from the posterior side of the phantom. In the oblique imaging (seated patient) position, the x-ray tube rotates from the cranium side of the phantom. Measurements using dedicated dental CBCTs were performed in the default (prone) position using 210° partial scan (Promax 3D MAX) and 360° full scan (i-CAT Next Generation). MSCT dose measurements were performed using a full 360° scan in (typical clinical) supine (lying patient) position. Philips Brilliance-64 and i-Cat effective doses were obtained in only one position. This was because 360° gantry rotation provides a symmetric dose profile in MSCT and CBCT devices and thus results in an equivalent dose distribution in all positions. The positioning of the acquisition volume in each case was assessed using a scout image acquired prior to the actual MSCT and CBCT exposures.

3.8. EFFECTIVE DOSE UNCERTAINTIES

The absorbed and effective dose uncertainties were evaluated based similarly on a previous study by Koivisto et al. (Koivisto 2013). The point dose measurement uncertainty was calculated as the weighted sum of variances and included the statistical measurement variations. The results were as follows: dosimeter and phantom positioning uncertainties (10%, 10%) (III), angular dependency variation (5%) (II), accumulated dose variation (4%) (I), x-ray source variation (5%) (IV), and cable irradiation uncertainties (1%) (Ehringfeld 2005).

4 RESULTS

4.1. CHARACTERIZATION OF MOSFET DOSIMETERS

4.1.1. PHOTON ENERGY DEPENDENCY

The MOSFET sensitivity measured using different filtrations was 3.10 ± 0.10 mV/mGy and 3.08 ± 0.14 mV/mGy using 2.5 mm Al and 2.5 mmAl+0.5 Cu filter combinations, respectively. The photon energy sensitivities (mV/mGy) and relative energy sensitivities using 2.5 mm Al filter and 2.5 mm Al + 0.5 mm Cu filter combinations with standard deviation (1SD) are presented in Fig. 4.1.1 and Fig. 4.1.2. The MOSFET dosimeter sensitivity was not statistically dependent on the chosen kVp or the filtration according to two-tailed Student's T-test ($p = 0.75$) and Pearsons correlation ($p_{Al} = 0.81$, $p_{Al+Cu} = 0.17$).

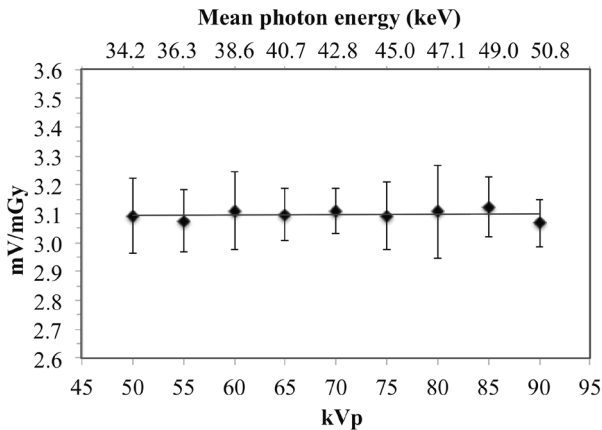


Fig. 4.1.1. MOSFET dosimeter sensitivity (mV/mGy) using a 2.5 mm Al filter (A) with corresponding error bars (1SD), ($y=0.0001 + 3.0882$, $R^2=0.00902$).

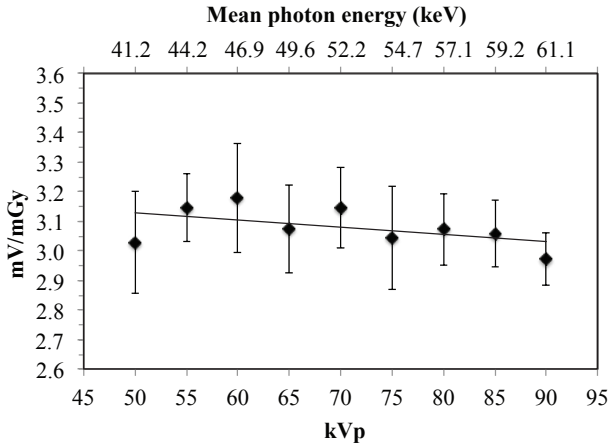


Fig. 4.1.2. MOSFET dosimeter sensitivity (mV/mGy) using a 2.5 mm Al + 0.5 mm Cu filter (B) with corresponding error bars (1SD), ($y=-0.024x + 3.2506$, $R^2=0.25435$).

4.1.2. DOSE, DOSE RATE, AND ACCUMULATED DOSE DEPENDENCIES

The MOSFET dosimeter dose dependency was insignificant with the following linear regression: $y=1.0030x + 0.0396$. The MOSFET dosimeters showed a good correlation with the MPD reference dosimeter ($R^2= 0.99987$). The standard deviation of the dose dependency measurements ranged from 2.4% to 12.5%. The MOSFET dosimeter dose rate sensitivity was 3.14 ± 0.11 mV/mGy for all evaluated dose rates (0.16 – 2.70 mGy/s). At 8.300 mV, the accumulated threshold voltage accumulated dose dependency was 3.10 ± 0.10 mV/mGy. At 17.500 mV, the accumulated threshold voltage calibration resulted in 2.83 ± 0.12 mV/mGy sensitivity. The average sensitivity decrease was 9.4 % over 9200 mV threshold voltage variation. The MOSFET sensitivity decrease rate caused by the accumulated dose was 1.02% per 1000 mV.

4.1.3. ANGULAR DEPENDENCY

The mean value and standard deviation of the measured sensitivity evaluated for PMMA for each rotation axis are presented in Table 5. The PMMA axial rotation measurements demonstrated a 5% standard deviation from the mean value (II).

Table 5. The mean and standard deviation of the measured sensitivity in PMMA

Material	Axial rot.(Ψ) (mV/mGy)	Normal to axial rot.(θ) (mV/mGy)	Tangent to axial rot.(φ) (mV/mGy)
PMMA	3.1 ± 0.1	3.3 ± 0.2	3.4 ± 0.2

4.1.4. MOSFET DOSIMETER UNCERTAINTY

The type A standard uncertainty ($Err(D)$) was assessed for six dose levels. The uncertainties of the ten repeated measurements were evaluated for each dose using 95% confidence interval (CI) ($k=2$). The combined uncertainty at 95% confidence interval at different doses were fitted into an exponential function and resulted in the following equation:

$$Err(D) = (0.285 * D^{-0.692} + 0.052) * n^{-0.5}, \quad (4)$$

where D is dose in (mGy) and n is the number of samples (exposures). The coefficient of determination was $R^2 = 0.99$. The single sample ($n = 1$) low dose limit for the MOSFET dosimeter was 1.7 mGy (Fig. 4.1.3). Furthermore, solving equation (4) for the number of samples (n) and the setting dose (D) to the TLD low-dose limit (0.3 mGy), according to Tarr et al and Dong et al. (Tarr 1998), (Dong 2002), resulted in a total of eight averaged MOSFET samples.

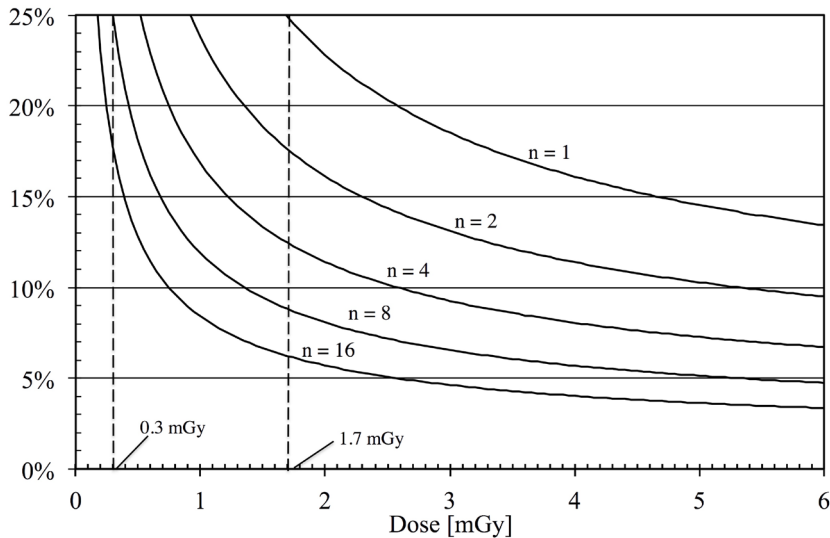


Fig. 4.1.3. The combined uncertainty (%) of MOSFET dosimeters as a function of dose and number of averaged samples ($n = 1-16$), 1.7 mGy one exposure low dose limit ($n=1$) and TLD comparable (0.3 mGy) low dose limit ($n=8$).

4.2. VALIDATION OF MOSFET DOSE MEASUREMENT METHOD

4.2.1. MOSFET MEASUREMENTS AND MONTE CARLO SIMULATIONS

MOSFET dose measurements: The imaging volume (dental area) used for the MOSFET dose measurements ranged from the tip of the chin to the sinuses (Z_{ref} of 83 cm) and is presented in Fig. 4.2.1.

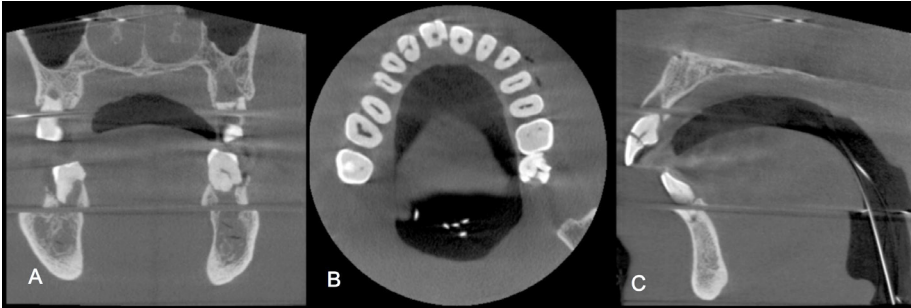


Fig. 4.2.1. Coronal (A), axial (B) and sagittal (C) views of the RANDO phantom (vertical positioning at Z_{ref} 83 cm as shown in Fig. 3.6.1).

The effective dose in the imaging volume was 153 μSv . The major contributions to the effective dose originated from the remainder tissues (32%), salivary glands (21%), and thyroid gland (21%). The greatest contributors to the effective dose in the remainder tissues dose were the oral mucosa (24%) and extrathoracic airways (7%).

The minimum and maximum effective dose in the typical imaging positions were 99 μSv (Z_{ref} of 84.5 cm) and 409 μSv (Z_{ref} of 78 cm), respectively. The effective dose contributions (μSv) of organs and the effective dose (μSv) determined in the RANDO phantom for Z_{ref} of 76 cm to 95 cm are presented in Fig. 4.2.2.

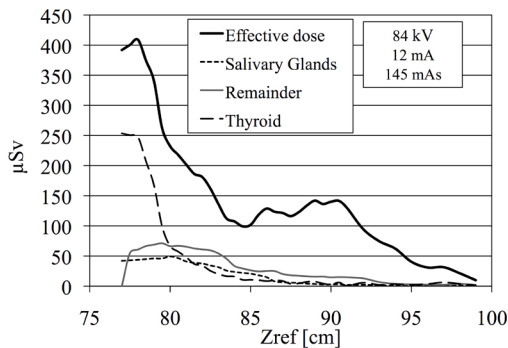


Fig. 4.2.2. Effective dose and effective dose contributions ($w_T H_T$) of some organs as a function of Z_{ref} in the RANDO phantom.

Absorbed dose uncertainty: The type A uncertainty of absorbed dose was dependent on the dose level. The average dose and uncertainty evaluated from ten repeated measurements of twenty dosimeters is presented in Table 6.

Table 6. The average of ten absorbed dose measurements and the dose uncertainty at the 95% confidence level

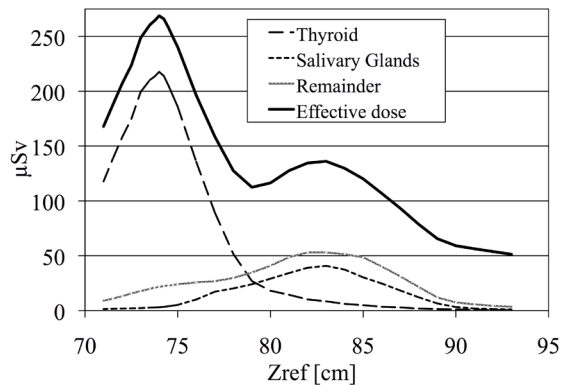
Dosimeter number	Dosimeter location in phantom	Measured Dose (mGy)	Dose uncertainty (%)
1	Calvarium anterior	0.17	36 %
2	Mid brain	0.2	31 %
3	Pituitary fossa	0.62	14 %
4	Right orbit	0.37	20 %
5	Right lens	0.27	25 %
6	Right cheek	3.34	6 %
7	Right ramus	4.77	5 %
8	Left ramus	5.27	5 %
9	Right parotid	4.35	5 %
10	Left parotid	4.53	5 %
11	Center C-spine	3.56	6 %
12	Left back neck	0.80	12 %
13	Right mandible body	1.58	8 %
14	Left mandible body	5.94	5 %
15	Right submandibular gland	5.37	5 %
16	Left submandibular gland	1.56	8 %
17	Center sublingula gland	1.58	8 %
18	Midline thyroid	0.97	11 %
19	Thyroid surface	0.67	13 %
20	Esophagus	0.79	12 %

Repeatability of MOSFET measurements: The RANDO phantom head was positioned in the CBCT x-ray centerline (Z_{ref} 83 cm). Repeatability calculations were performed by comparing the results of two measurements, including a new phantom placement, both consisting of the average doses of ten identical scans. Effective dose, organ dose contributions, and the variation percentage of measurement 1 and measurement 2 are presented in Table 7.

Table 7. Repeatability of measurements of ICRP 103 effective dose and the contributions ($w_T H_T$) of various organ doses to the effective dose in the standard dental imaging case

Organs	Meas. 1 (μSv)	Meas. 2 (μSv)	Difference %
Salivary Glands	32.1	31.6	1.5%
Thyroid	32.0	32.8	-2.5%
Bone Marrow	24.7	25.2	-2.1%
Bone Surface	6.5	6.6	-2.1%
Esophagus	2.9	3.2	-7.1%
Brain	4.3	4.1	4.0%
Skin	0.7	0.7	-2.2%
Remainder	49.3	49.0	0.8%
Lymphatic nodes	1.5	1.5	1.5%
Extrathoracic airways	10.1	10.5	-3.8%
Muscle	1.2	1.1	1.4%
Oral mucosa	36.6	35.8	2.1%
Effective dose	152.5	153.2	-0.4%

Monte-Carlo simulations: MC simulations resulted in $136 \mu\text{Sv}$ for the Z_{ref} of 83 cm. The largest contributions to the effective dose by MC simulations were from the remainder tissues (40%), salivary glands (31%), bone marrow (14%), and thyroid gland (6%). The overall effective dose variation in the measured height range was from $112 \mu\text{Sv}$ (Z_{ref} of 79 cm) to $269 \mu\text{Sv}$ (Z_{ref} of 74.0 cm). Fig. 4.2.3 shows the effective dose contributions of various organs and the effective dose as a function of Z_{ref} as obtained from the MC simulations.

**Fig. 4.2.3.** Simulated effective dose and effective dose contributions of some organs as a function of Z_{ref}

Dose comparison: Table 8 presents the effective dose comparison at Z_{ref} of 83.0 cm. A comparison was made between 20 averaged MOSFET dose measurements (Meas. 1 and Meas. 2 in Table 7) and MC simulation results.

Table 8. MOSFET and Monte-Carlo estimates of effective dose and dose contributions of various organs in the standard dental imaging case

Organs	MOSFET (μSv)	MC (μSv)	Difference %
Salivary Glands	32	41	-22%
Thyroid	32	8.4	280%
Bone Marrow	25	18	40%
Bone Surface	6.5	6.9	-5.4%
Esophagus	3.0	0.4	600%
Brain	4.2	2.8	51%
Skin	0.7	1.0	-25%
Remainder	49	53	-7.3%
Effective dose	153	131	17%

4.2.2. MOSFET AND TLD COMPARISONS

The TLD effective doses ranged between 7.0 and 158.0 μSv and the MOSFETs doses between 6.1 and 175.0 μSv . The effective doses and the correlation coefficients (cc) are presented in Table 9. In addition, the effective dose and the organ dose contributions of radiosensitive organs, the difference percentages between the results, and the fractions of the effective dose obtained using MOSFET and TLD dosimeters of protocol no. 1 are presented in Table 10.

Table 9. Effective doses (Qsv), difference percentages and correlation coefficients (cc) attained using thermoluminescent dosimeter (TLD) (TLD 100, Thermo Fisher Scientific, Waltham, MA) and metal oxide semiconductor field-effect transistor (MOSFET) dosimeters using four different CBCT protocols

Number	Protocol	FOV (cm)	TLD (μSv)	MOSFET (μSv)	Difference (%)	cc
1	Face, maxillofacial	20 x 17	87,6	83,4	-5	0.99636
2	Teeth , upper jaw	8.5 x 5	7,0	6,1	-14	0.80801
3	Tooth, mandible	4 x 5	12,3	10,3	-16	0.98760
4	Teeth, both jaws	10 x 10	158,2	174,9	11	0.98994

Table 10 MOSFET and TLD estimates of effective dose (QSv), dose contributions, and fraction (%) of effective dose in Face (maxillofacial) FOV 20 x 17 cm protocol

	MOSFET (μSv)	TLD (μSv)	Difference (%)	MOSFET fraction	TLD Fraction
Bone Marrow	24.2	24.6	-2 %	29 %	28 %
Thyroid	11.4	11.4	0 %	14 %	13 %
Esophagus	1.2	1.3	-12 %	1 %	2 %
Skin	0.7	0.7	-3 %	1 %	1 %
Bone surface	2.0	2.0	-2 %	2 %	2 %
Salivary glands	10.6	10.4	2 %	13 %	12 %
Brain	12.2	13.2	-8 %	15 %	15 %
Remainder	21.2	24.0	-12 %	25 %	27 %
Lymphatic nodes	0.5	0.5	-7 %	1 %	1 %
Extrathor. airways	10.5	11.9	-12 %	13 %	14 %
Muscle	0.5	0.5	-11 %	1 %	1 %
Oral mucosa	9.8	11.0	-11 %	12 %	13 %
Effective dose	83.4	87.6	-5 %	100 %	100 %

Source variation: The CBCT source variation uncertainty was evaluated using two identical CBCT devices and the same full-face protocol 1 (face, maxillofacial; FOV, 20 x 17 cm). The effective doses were 87.2 and 83.3 μSv resulting in a source variation of 5% (IV).

4.3. EFFECTIVE DOSES OBTAINED USING ONE MDCT DEVICE AND THREE CBCT DEVICES

Table 11 presents the effective dose and organ dose contributions of the most radiosensitive organs to the effective doses for the Planmed Verity CBCT scanner, the Promax 3D MAX, the i-CAT Next generation, and the Philips Brilliance 64 MSCT devices.

Table 11. ICRP 103 effective doses (Q_{Sv}) and organ dose contributions (wTHT) of various organ doses to the effective dose for CBCT and MSCT scanners

Organ	Planmed Verity (210°)			Promax 3D MAX	i-Cat Next Gen.	Philips Brilliance-64
	Oblique	Prone	Supine	Prone (210°)	(360°)	(360°)
Bone Marrow	40.5	48.1	68.4	42.7	49.7	158
Thyroid	16.6	27.8	48.1	16.4	22.0	261
Esophagus	1.6	3.5	4.3	2.1	2.4	25.4
Skin	0.9	1.1	1.9	0.9	1.1	4.3
Bone surface	10.6	12.6	17.9	3.6	13.0	41.4
Salivary glands	14.6	25.4	30.4	32.0	21.6	82.7
Brain	26.6	26.0	21.1	20.4	23.2	68.3
Remainder	22.7	47.2	54.9	49.7	36.9	140
Lymphatic nodes	0.7	1.2	1.4	1.5	1.0	3.8
Extrathoracic airw.	7.7	14.2	18.1	16.5	12.1	54.2
Muscle	0.6	1.2	1.5	1.4	1.0	4.0
Oral mucosa	13.8	30.6	33.9	30.3	22.8	78.0
Effective dose	134	192	247	168	170	781

4.4. EFFECTIVE DOSE UNCERTAINTIES

The combined measurement uncertainty, e.g. in the Face (FOV 20 x 17) protocol for a single dosimeter, varied between 16 and 21%. The tissue dose uncertainty was dependent on the dosimeter uncertainty and the estimated uncertainty of the fraction irradiated f_i (25%). The tissue dose uncertainties of bone marrow, thyroid gland, esophagus, skin, bone surface, salivary glands, and brain were 25%, 24%, 34%, 20%, 25%, 20%, and 21%, respectively. For the remainder tissues, the tissue uncertainties for lymphatic nodes, extrathoracic airways, muscles, and oral mucosa were 14%, 18%, 14%, and 10%, respectively. The expanded effective dose uncertainties (2SD) were calculated as a weighted sum of the variances of all tissues. The results for the measured protocols were as follows: 20% for “Face” (FOV 20 x 17), 66% for “Teeth upper jaw” (8.5 x 5), 22% for “Teeth both jaws” (FOV 10 x 10 cm), and 42% for “Tooth mandible left molar” (FOV 4 x 5 cm). The combined uncertainties for all devices used in this study are presented in publications (III, IV, V)

5 DISCUSSION

Since their introduction into maxillofacial imaging in 1997, CBCTs have become widely used by dentists and oral and maxillofacial surgeons (Ganguly 2009). To date, several methods have been proposed to reduce the effective doses in CBCT devices (Yu 2009).

An awareness of the radiation risks has consequently led to the development of novel CBCT devices with decreased radiation output. At present, the most common method of reducing the effective dose is to reduce exposure parameters and the field of view. Moreover, the effective doses can be further reduced on CBCT devices with the addition of filtration that subsequently removes the lower energy spectra that contributes to the effective dose without improving image quality. Despite the tendency towards developing x-ray devices that produce lower effective doses, the radiation lifetime risk still remains difficult to assess. Therefore, newer, faster, and more effective methods for effective dose assessment are needed.

Traditional TLD measurement methods using anthropomorphic phantoms take approximately 1.5-2 hours to accomplish resulting in a maximum of 4-5 protocol measurements per working day. Since modern day CBCT devices can have up to 330 (Promax 3D MID) exposure protocols, several weeks of measurements are consequently required. By using MOSFET dosimeters, however, one dose measurement cycle takes only approximately two minutes. Therefore, depending on the required number of repetitions needed, a maximum of 80 protocols per working day can be measured. The MOSFET setup presented in this study provides a significant improvement in terms of time and effort, when compared with traditional TLDs.

The first aim of this thesis was to characterize MOSFET dosimeter sensitivity, energy, dose, and angular dependencies in order to assess the suitability of MOSFET dosimeters for low-dose CBCT measurements in anthropomorphic phantoms. A second aim was to develop and to validate a dose measurement system for effective dose assessment in anthropomorphic phantoms using Monte Carlo simulations and TLD measurements. The third aim was to apply the newly developed measurement system to assess the effective doses resulting from three CBCT and one MSCT device.

5.1 MOSFET DOSIMETER CHARACTERIZATION FOR DOSE DEPENDENCIES

MOSFET dosimeters were characterized for CBCT photon energy ranges, dose properties, angular sensitivity, and dose uncertainties in studies I and II.

The energy dependency results of this study demonstrated that MOSFET dosimeter sensitivity was statistically independent of the mean photon energy ranges (34.2 – 50.8 keV, 41.2 – 61.1 keV), that were attained using two filter combinations and tube potentials between 50 kVp and 90 kVp.

A recent study by Manninen et al. (Manninen 2014a), investigated MOSFET (TN-1002RD) energy dependency using tube potentials between 40 kVp and 125 kVp. Compared with the reference dosimeter value, they observed a 6% coefficient of variation for tube potentials between 60 and 110 kVp: a -10% decrease at 40 kVp and a -14.6% decrease at 125 kVp, respectively. These differences are explained by the lower number of exposures applied (5 versus 10), the lower dose (5 mGy versus 17 mGy/20 mGy), which affected the uncertainty, different mean photon energy (keV) range and finally by the different thickness (10 mm) of the backscatter material that was used in their study. Likewise, another factor that could help explain the differences may have been the different dosimeter attenuation characteristics caused by the reinforcement of the dosimeter type (TN-1002RD-H) used in this study.

In an earlier study by Dong et al. (Dong 2002), the photon energy response of MOSFET dosimeters was evaluated for skin dose measurements using tube voltages between 40 and 125 kVp ($E_{ave} = 26.5 - 39.7$ keV). Their study resulted in a 20% decrease in sensitivity from 40 kVp to 90 kVp. The different energy range and the water backscatter material used by Dong et al. may well explain the differences when compared to the statistically insignificant sensitivity variations observed in our study. Furthermore, a study by Peet et al. (Peet 1999) evaluated the energy sensitivity of MOSFETs over a range of 60 – 100 kVp for diagnostic purposes. The photon energy sensitivity varied between 2.2 mV/mGy – 2.9 mV/mGy. The results of their study showed -20% lower sensitivity at 60 kVp compared with the (normalized) 90 kVp value. The lower sensitivity results may also have been caused by the different orientation of the MOSFET epoxy bulbs that faced towards the water backscatter material. In this thesis, the epoxy bulbs were directed towards the x-ray source to attain the highest sensitivity based on a previous study by Koivisto et al. (II).

In a previous study Bower et al. (Bower 1998) characterized MOSFET dosimeter energy dependency using a (roughly) constant dose and a tube voltage ranging between 40 – 140 kVp. Their choice of the constant dose, PMMA backscatter material, and ionization chamber reference dosimeter resulted in comparable values to those attained in our study when the results of both studies were normalized to 90 kVp tube voltage.

In this thesis the MOSFET dosimeter dose dependency (linearity) was evaluated using a dose range of 0.24–17.5 mGy. The results demonstrated that MOSFET dosimeters can be used without dose dependency correction factors for low dose (0.24–17.5 mGy) measurements. The results were comparable with the findings of Dong et al. (Dong 2002) and Bower et al. (Bower 1998).

The MOSFET dose rate dependency was assessed using 0.16 – 2.70 mGy/s dose rates. No statistically significant variation in the sensitivity at different dose rates was observed, and therefore no dose rate correction was needed (Izewska 2005).

The MOSFET dosimeter sensitivity was assessed as a function of the accumulated dose over a 9.200 mV threshold voltage range. This resulted in a 1% decrease of sensitivity per 1000 mV threshold voltage, which is in good agreement with the findings of Brady et al. (Brady 2012) and Toncheva et al. (Toncheva 2010). The point doses obtained in the anthropomorphic RANDO phantom using MOSFET dosimeters resulted in a (-8%) lower average point dose (1.10 mGy) value than that obtained using TLD dosimeters (1.19 mGy). This (-8%) difference can be explained by a loss of MOSFET sensitivity previously described Brady et al. (Brady 2012) ($\approx 1\%$ per 1000 mV) and Toncheva et al. (Toncheva 2010) ($\approx 3\%$ per 3000 mV) and by the (≈ 9200 mV) increase in the accumulated threshold voltage between the calibration and the phantom measurements.

The dosimeter (1SD) uncertainties in the phantom measurements ranged between 26% (0.24 mGy) and 7% (2.29 mGy) using 10 averaged samples. Furthermore, the combined (point dose) (1SD) uncertainty, calculated as the weighted sum of variances ranged between 17% and 30%. All TLD and MOSFET point dose values except for those in the left and right submandibular glands were within the range covered by the extended (2SD) combined MOSFET uncertainty (U_c). The higher MOSFET doses observed in the left and right submandibular glands could be due to the vertical position variations of the dosimeters in their designated phantom holes: the surrounding mandible bones may have also caused different attenuation and scatter profiles to the dosimeters.

5.2. MOSFET DOSIMETER UNCERTAINTY

In this thesis the MOSFET dosimeter uncertainty was evaluated to define the single sample low-dose limit (25% uncertainty, $k=2$) and to assess the number of exposures needed to attain the previously proposed TLD (1 exposure) low-dose (0.3 mGy) limit. The purpose of this study was to also assess the MOSFET sensitivity for different energy ranges and to compare the MOSFET point dose results with those obtained using TLDs.

According to the findings of this thesis, the TLD comparable low dose limit (0.3 mGy) can be achieved by averaging eight MOSFET exposures. When comparing the single-sample, low-dose detection limit of MOSFET dosimeters (1.40 mGy) attained by Yoshizumi et al. (Yoshizumi 2007) with the dose obtained in this study (1.69 mGy), the results showed a 21% higher dose value. The difference in results could be caused by MOSFET sensitivity decrease due to a higher 120 kVp compared to the 80 kVp used in this study. In a prior study performed by Peet et al. (Peet 1999), the observed minimum (25% total uncertainty, $k=2$) dose was 1.5 mGy when MOSFET detectors were evaluated for entrance surface dose measurements. Their 11% lower value could have been caused by the water backscatter material which has a lower backscatter factor (BSF) than the PMMA used in this study.

5.3. VALIDATION OF THE MOSFET DOSE MEASUREMENT SETUP

Monte-Carlo simulation: A novel mobile MOSFET dosimetry setup was developed and used to determine organ and effective dose in the maxillofacial area using an anthropomorphic RANDO head phantom. The purpose was also to compare the experimental MOSFET results with Monte Carlo (MC) simulations.

In the standard dental imaging mode (Z_{ref} of 83 cm), the observed difference between the effective dose obtained using 20 MOSFET dosimeters and the corresponding MC simulations was relatively small, 17%. The effective dose difference was between $\pm 25\%$ for Z_{ref} from 82 cm to 87 cm covering the most commonly used maxillofacial imaging regions. The differences between simulations and measurements can be explained by the differences in the mathematically modeled and physically realized phantoms, the necessity of having to rely on a limited number of 20 point measurements, and the method of assessing organ doses based on the measurements. Furthermore the differences in the thyroid gland and esophagus effective dose contributions obtained using MOSFET dosimeters and Monte Carlo simulations (Table 8) can be explained by the differences in the organ positions in relation to the exposed volume which subsequently had a minor effect to the effective dose.

The findings in this study demonstrate that individual patient anatomy and positioning have a drastic effect on the overall effective dose. The area most affected by the vertical positioning of the beam was the transition zone between the lower part of the oral cavity and the thyroid gland. A minor change in patient positioning in the designated area subsequently increased the dose by 16% (III).

Another observation was that there seems to be an optimal height both in the

physical phantom and in the Cristy-Eckerman model where the effective dose has a minimum value. This information may be useful for dose reduction when using 8 x 8 cm imaging volume. The positioning of patients to an x-ray beam is a decision that is based on clinical needs. It is, however, especially important to avoid any exposure of the thyroid gland region because exposure to this area rapidly increases the effective dose.

MOSFET-TLD: In this thesis the MOSFET dose measurement setup was validated for effective dose assessment in the maxillofacial region. This was accomplished by comparing MOSFET results to TLD reference values obtained in identical conditions.

To date, TLDs are the most commonly used dosimeters in dose measurement studies due to their sensitivity and small size (Davis 2003). Furthermore, TLDs are often used for effective dose assessments (Ludlow 2003), (Ludlow 2006), (Roberts 2009), (Suomalainen 2009), (Rottke 2013). Nevertheless, TLDs have certain limitations especially when a small number of dosimeters are used in point-dose measurements (Pauwels 2010). TLDs and MOSFETs are sensitive to phantom tilting (III), and therefore minor shifts in the FOV can have a significant impact on the effective dose results (IV). Previous studies using TLDs have also reported differences between the x-ray sources, phantoms, phantom positioning, and placement of the dosimeters in the phantoms.

In order to minimize the above discussed dosimeter limitations, the following precautions were undertaken in this thesis: all measurements were performed using the same CBCT device to minimize the source variations; only one anthropomorphic phantom was used in this study offering equal attenuation and scattering conditions; identical TLD and MOSFET dosimeter positions were used in the phantom head; the phantom head was specially fixed to the CBCT device to allow exact repositioning after replacing the dosimeters in the phantom. In addition, the positioning of the acquisition volume in each case was verified using a reconstructed 3D image of the anatomical structures in the FOV.

In order to avoid any inaccuracies induced by the limited number of exposed dosimeters in the small FOV, the organ dose contributions were assessed using the full-face protocol no. 1 (Face, maxillofacial, FOV 20 x 17 cm). The large FOV protocol yielded 5% less effective dose values in the MOSFETs when compared with the TLDs. The largest differences in the effective dose contributions were measured in the remainder tissues (-12%) and esophagus (-12%). These differences could be due to minor variations in the phantom positioning, as previously discussed.

When comparing the effective doses acquired using protocol no. 2 (teeth upper jaw, FOV 8.5 x 5 cm), the MOSFET dosimeters recorded 14% lower effective dose (6.1 μ Sv) values than the TLD dosimeters (7.0 μ Sv). The largest difference between MOSFET and TLD measurements were observed in the thyroid gland (MOSFET: 1.5

μSv , TLD: $0.7 \mu\text{Sv}$; +121%). The largest difference in the effective dose contribution was attained in the remainder tissues (MOSFET: $1.9 \mu\text{Sv}$, TLD: $3.0 \mu\text{Sv}$; -36%). The higher effective dose observed in the thyroid gland and the lower values attained in the remainder tissues are possibly due to the unintended vertical shifting of the FOV position between different TLD and MOSFET measurements.

The limited number of dosimeters used in this study and the uncertainty of the doses measured near the x-ray field edge may have caused the differences in the small FOV results. Pauwels et al. have previously observed this phenomenon (Pauwels 2010). The greatest effective dose contribution difference was observed in the thyroid gland. When comparing the source variation using two CBCT devices, only minor differences of 5% in the effective doses were observed. This could be an indication of position differences between two MOSFET set-ups. However, it must be noted that the mean effective dose variation between the measured protocols using MOSFET and TLD methods was only 2%.

5.4. MOSFET DOSE MEASUREMENT SETUP APPLICATION

In the present study, organ and effective doses were assessed in three different phantom head positions using a Planmed Verity CBCT scanner that has recently been approved for maxillofacial imaging. The device uses a partial 210° gantry scan and generates an asymmetric and non-equivalent dose distribution in the phantom head that makes it necessary to assess the effective dose in different positions. The Planmed Verity effective doses obtained in the supine position were 29% higher ($247 \mu\text{Sv}$) than those obtained in the prone position ($192 \mu\text{Sv}$). Furthermore, when the prone and oblique positions were compared, the effective dose in the oblique position was 30% lower.

When compared with the dental reference CBCT in the prone position, the Planmed Verity CBCT scanner yielded a 14% higher effective dose compared with the Promax 3D MAX. The difference ($24 \mu\text{Sv}$) can be well explained by the larger field of view and the smaller focus-to-target distance of the Planmed Verity CBCT scanner. The contributions of organs to the effective dose between the devices were, however, different. More specifically, when exposed using the Planmed Verity CBCT scanner, the thyroid gland and the bone surface presented slightly higher organ doses than those of the Promax 3D MAX and subsequently demonstrates the differences in the imaging geometry and FOV size.

Another reference effective dose ($170 \mu\text{Sv}$) for comparison in the prone position was attained using an i-Cat Next Generation CBCT device. In the comparison, the Planmed Verity CBCT scanner resulted in a 13% higher effective dose. The difference is mainly due to the effective dose contributions in the thyroid gland,

salivary glands, and remainder tissues. In this study, the effective dose for the i-Cat Next Generation CBCT device was obtained in the high-resolution mode (170 μSv , 120 kVp, 37 mAs) that is found to double the effective dose⁴. The obtained value is comparable, when scaled by current-exposure-time product, to the results of previous studies by Pauwels (Pauwels 2010) et al. (83 μSv , 120 kVp, 18.5 mAs) and Ludlow et al. (Ludlow 2008) (87 μSv , 120 kVp, 19 mAs).

Finally, effective doses were assessed using a MSCT device resulting in an effective dose of 781 μS . In a previous study by Loubele et al. (Loubele 2008), the MSCT effective dose varied between 995 μSv and 1160 μSv . These results were, however, obtained using a 22.5 cm scan length while the scan length used in this study was 18 cm. In order to compare our results with the previous studies, we scaled down the scan length from 22.5 cm to 18 cm resulting in effective doses between 796 μSv and 928 μSv . These were, however, between 2% to 19% higher than the 781 μSv of this study.

There are certain limitations in this thesis. The limited number of dosimeters used in this thesis could be a potential source of error. In a recent study by Pauwels (Pauwels 2013) that focused on the impact of dosimeter quantity on the effective dose assessment, it was demonstrated that a large number of dosimeters are needed for accurate dose estimation in particular for red bone marrow, thyroid gland, salivary glands, and remainder tissues.

Another possible source of error in this study were the differences in the estimated irradiated organ fractions. The estimated amount of bone marrow (Cristy 1987) was also a potential source of error when the age-dependent variations of bone marrow are considered. A further weakness of this study is that the thyroid gland may not be fully contained in phantom layer 9 (Fig. 3.3.1) but in the lower layers 10 and 11, which may have caused an error in the dose assessment.

Therefore, an interpretation of the results should be carried out with care since the results were obtained using the manufacturer-recommended imaging parameters without taking image quality in terms of contrast, noise sharpness, or diagnostic value into account.

5.5. FUTURE DEVELOPMENTS IN EFFECTIVE DOSE ASSESSMENT

The accuracy of the MOSFET dose assessment setup developed in this thesis could be further improved by increasing the number of dosimeters to around 150 as proposed by Pauwels et al. (Pauwels 2010). An increased number of dosimeters is especially important in small FOVs where the subsequent number of dosimeters is limited. To date, the MOSFET dosimeter flexible wire has a limited length of 200

mm, which subsequently restricts the positioning of dosimeters in the upper part of the phantom. Furthermore, in the present setting, the number of cables that can be routed through the phantom base are limited to 20 dosimeter cables due to the size of the entry void. These shortcomings can be improved by increasing the length of the flexible wire to approximately 300 mm to allow for the placement of the dosimeters in the cranial area.

To date, the MOSFET software used in this study allows individual dosimeter calibration coefficient adjustment. However, the results of this study and the findings of Brady et al. (Brady 2012) and Toncheva et al. (Toncheva 2010) showed that in order to improve the accuracy there is need for user-adjustable, cumulative dose correction coefficient. Such a correction coefficient could be implemented into the TN-RD-75M software used in this study.

Although MOSFET dosimeters are easy to use, they have a limited life expectancy. Therefore, alternative electronic dosimeters with infinite lifespans should be developed.

The different absorbed dose profiles attained within the phantom using different vertical patient positions (III) and CBCT scan directions (V) revealed new possibilities for dose reduction that should be further investigated.

6 CONCLUSIONS

In this thesis, a real time low-dose measurement setup using MOSFET dosimeters was developed to match the growing need for the assessment of effective doses in the increasing number of dental CBCT devices and protocols used worldwide. Moreover, the novel setup developed in this thesis can be applied in hospitals and other clinical settings to monitor the protocol-specific effective doses induced by different dental CBCTs.

The MOSFET dosimeter characterization presented good dose linearity and statistically insignificant energy dependency for the investigated dental energies. However, due to their variation in angular sensitivity, MOSFET dosimeters should always be calibrated in the actual clinical settings for the beam geometry and angular range of the CBCT exposure. The results of the validation procedure confirmed that the developed MOSFET dose measurement setup is capable of producing similar results to those attained using the MC simulation program. Furthermore, when taking into account the uncertainties of TLD and MOSFET measurement methods and the results of the statistical analysis, the effective doses acquired using MOSFET dosimeters were found to be in good agreement with those obtained using TLD dosimeters. When compared with the previously used methods, the major benefit of the setup developed in this thesis is its ability to acquire the effective dose values in a fraction of the time needed when using TLDs. Such an increase in effective dose acquisition speed makes the extensive series of CBCT dose measurements in anthropomorphic phantoms feasible.

In future, there will be a growing tendency to perform the effective dose assessment using simulations that are based on 3D models. The MOSFET setup presented in this thesis with its point dose values will serve as an excellent validation method for such future developments.

In summary, the fast and dependable low dose measurement setup developed and presented in this thesis provides an effective means of CBCT dose assessment using a variety of dental protocols.

7 ACKNOWLEDGEMENTS

This doctoral thesis presents the work that was carried out under the supervision of the Department of Physics at the University of Helsinki between 2010 and 2015.

First of all, I would like to offer my sincere thanks to my principal supervisor Professor Sauli Savolainen. A brief meeting with him in August 2010 became the starting point of this thesis. I am extremely grateful for having had the excellent opportunity to complete the scientific work under his supervision.

I am also indebted to Ph.D., Docent, Chief Physicist Mika Kortensniemi at Helsinki University Hospital for his guidance and support in the carrying out of this thesis.

I am especially grateful to Dr. med. Dent. Jan Wolff who visited the Planmeca research laboratory in summer 2010 to see the newly developed dose measurement setup. He immediately understood the value of the work and proposed that I prepare publications on the topic. Moreover, I am most appreciative for his guidance, consistent support, and the enormous number of hours of conversation we had during the carrying out of this thesis.

I am grateful to the co-authors of the related publications. Special thanks are due to Timo Kiljunen, Ph.D., Dirk Schulze, Ph.D., and Markku Tapiovaara, MSc., for their professional reviews and constructive comments on the publications that have led to a markedly improved thesis.

I wish to thank the official reviewers of the thesis, Professor Miika Nieminen, Ph.D. and Docent Simo Saarakkala, Ph.D. for their constructive remarks. I would also like to thank Peter Heath MA for revising the language of the manuscript.

I am indebted to a number of friends and colleagues who took the time to listen and encourage me during the process.

I am very grateful to Heikki Kyöstilä, President of Planmeca Oy, Vice Presidents Arto Virta, M.Sc., Timo Müller, M.Sc., and Helianna Puhlin-Nurminen, M.Sc. who have supported this work from the beginning and who granted permission for the MOSFET dose measurement project to be established in April 2009. Planmeca Oy is acknowledged for the financial support given for this work.

I express my warmest appreciation to my parents for their endless support and encouragement they have given me throughout my life.

I want to especially express my deepest gratitude to my family who have been very considerate, patient, and understanding during the time it took to complete this study.

Juha Koivisto

Helsinki, Finland
25th of August 2015

REFERENCES

- Akselrod, MS, and Akselrod AE. "New $\text{Al}_2\text{O}_3:\text{C}$, Mg crystals for radiophotoluminescent dosimetry and optical imaging." *Radiation protection dosimetry* 119.1-4 (2006): 218-221.
- Arai Y, Tammissalo E, Iwai K, Hashimoto K, Shinoda K. Development of a compact computed tomographic apparatus for dental use. *Dentomaxillofac Radiol* 28:245-248, 1999.
- Aschan, C. (1999). *Applicability of thermoluminescent dosimeters in X-ray organ dose determination and in the dosimetry of systemic and boron neutron capture radiotherapy*. Helsinki: University of Helsinki.
- Birch R and Marshall M. Computation of bremsstrahlung x-ray spectra and comparison with spectra measured with a Ge(Li) detector, *Physics in Medicine Biology* 1979; 24; 505.
- Bower MW, Hinterlang HE. The characterization of a commercial MOSFET dosimeter system for use in diagnostic X-ray. *Health Phys.* 1998 Aug;75(2) 197-204
- Boone JM. The trouble with CTDI₁₀₀. *Med Phys.* 2007;34:1364-1371.
- Brady SL, Kaufmann RA. Establishing a standard calibration methodology for MOSFET detectors in computed tomography dosimetry. *Med. Phys.* 2012;39(6), 3031-40.
- Briere TM Tailor R, Tolani N, Prado K, Lane R, Woo S, Ha C, Gillin MT, Beddar AS., Patient dosimetry for total body irradiation using single-use MOSFET detectors. *J Appl Clin Med Phys.* 2008 Nov 3;9(4):2787.
- Büerman L, Böttcher R. Performance test of multi-parameter measuring devices used for quality assurance in diagnostic radiology. IAEA. Proceedings of an International Symposium Vienna. Vol 2. 2010 pp. 41
- Cristy M, Eckerman KF. Specific absorbed fractions of energy at various ages from internal photon sources. I. Methods. report ornl/TM-8381/V1. oak ridge: oak ridge national laboratory; 1987.
- Davis SD, Ross CK, Mobit PN, Van der Zwan L, Chase WJ and Shortt KR. "The response of lif thermoluminescence dosimeters to photon beams in the energy range from 30 kV x rays to 60Co gamma rays." *Radiation Protection Dosimetry* Vol. 106, No. 1, pp. 33-43 (2003)
- Dawood A, Patel S, Brown J. Cone beam CT in dental practice. *Br Dent J* 2009; 207: 23-28.

- Dong SL, Chu TC, Lan GY, Wu TH, Lin YC, Lee JS. Characterization of high-sensitivity metal oxide semiconductor field effect transistor dosimeters system and LiF:Mg,Cu,P thermoluminescence dosimeters for use in diagnostic radiology; *Applied Radiation and Isotopes* 57 (2002) 883–891
- Draenert FG, Coppenrath E, Herzog P, Müller S, Mueller-Lisse UG. Beam hardening artefacts occur in dental implant scans with the NewTom cone beam CT but not with the dental 4-row multidetector CT. *Dentomaxillofac Radiol.* 2007 May;36(4):198–203.
- Ehringfeld C, Schmid S, Poljanc K, Kirisits C, Aiginger H, Georg D. Application of commercial MOSFET detectors for in vivo dosimetry in the therapeutic x-ray range from 80 kV to 250 kV. *Phys Med Biol.* 2005;50(2):289–303.
- Feldkamp LA, Davis LC, Kress JW. Practical cone-beam algorithm. *J Opt Soc Am* 1984; A1(6):612–9.
- Ganguly R. Accuracy of linear measurement in Galileos cone beam CT under simulated clinical condition. Thesis, University of Iowa, 2009
- He W, Huda W, Magill D, Tavriles E, Yao H. Patient doses and projection angle in cone beam CT. *Med Phys.* 2010 May; 37(5):2359–68.
- Holroyd, JR. and Walker, A. Recommendations for the design of X-ray facilities and the quality assurance of dental cone beam CT (computed tomography) systems. A Report of the HPA Working Party on dental cone beam CT. HPA-RPD-065. Health Protection Agency (2010).
- International Atomic Energy Agency, 2007. Dosimetry in Diagnostic Radiology: An International Code of Practice. IAEA, Vienna (Technical Report Series No. 457).
- International Commission on Radiation Units and Measurements, Radiation quantities and units, ICRU Rep. 33, ICRU Publications, Bethesda, Maryland (1980).
- International commission on Radiation Units and Measurements (ICRU). Patient dosimetry for x-rays used in medical imaging. Report No. 74. *Journal of the ICRU* 2005; 5 (2).
- Implications of Commission Recommendations that Doses be Kept as Low as Readily Achievable. ICRP Publication 22. Pergamon Press, Oxford.
- International commission on Radiological Protection (ICRP). 1990 Recommendations of the ICRP. ICRP Publication 60. *Ann ICRP* 1991; 21:1-201.
- International commission on Radiological Protection (ICRP). Recommendations of the ICRP. ICRP Publication 103. *Ann ICRP* 2008; 37:2–4.
- Izewska, J. and Rajan, G. (2005) Chapter 3: Radiation Dosimeters. In: Podgorsak, E.B., Ed., *Radiation Oncology Physics: A Handbook for Teachers and Students*, International Atomic Energy Agency-IAEA, Vienna.

- Jaju PP, Jaju SP, Clinical utility of dental cone-beam computed tomography: current perspectives. *Clinical, Cosmetic and Investigational Dentistry* 2014;6 29–43.
- Kahng, Dawon, “Electric Field Controlled Semiconductor Device,” *U. S. Patent No. 3,102,230* (Filed 31 May 31, 1960, issued August 27, 1963).
- Kau CH, Richmond S, Paloma JM, Hans MG. Three-dimensional cone beam computerized tomography in orthodontics. *J Orthod.* 2005 Dec;32(4):282–93.
- Khan F. *The Physics of Radiation Therapy*, Third Edition. Lippincott Williams & Wilkins. 2003.
- Kiljunen, T. Patient doses in CT, dental cone beam CT and projection radiography in Finland, with emphasis on paediatric patients. *STUK-A232*, 62 pp.+apps.66 pp (2008).
- Kim S, Yoshizumi TT, Frush DP, Toncheva G, Yin FF. Radiation dose from cone beam CT in a pediatric phantom: risk estimation of cancer incidence. *AJR Am J Roentgenol.* 2010a Jan;194(1):186–90.
- Kim S, Yoshizumi TT, Toncheva G, Frush DP, Yin FF. Estimation of absorbed doses from paediatric cone-beam CT scans: MOSFET measurements and Monte Carlo simulations. *Radiat Prot Dosimetry.* 2010b Mar;138(3):257–63.
- Kim S, Song H, Samei E, Yin F and Yoshizumi TT. Computed tomography dose index and dose length product for cone-beam CT: Monte Carlo simulations of a commercial system *Journal of Applied Clinical Medical Physics*, Vol. 12, No. 2, Spring 2011a.
- Kim S, Sopko D, Toncheva G, Enterline D, Keijzers B, Yoshizumi TT. Radiation dose from 3D rotational X-ray imaging: organ and effective dose with conversion factors. *Radiat Prot Dosimetry.* *Radiat Prot Dosimetry* (2011b) doi: 10.1093/rpd/ncr369
- Kohno R, Nishio T, Miyagishi T, Hirano E, Hotta K, Kawashima M, Ogino T, “Experimental evaluation of a MOSFET dosimeter for proton dose measurements”, *Phys. Med. Biol.* 51, 2006, pp. 6077–6086.
- Kouno, T, Araki, F, Nakaguchi, Y, Oono, T. Dose distribution from kV-cone beam computed tomography in image-guided radiotherapy. *Nihon Hoshasen Gijutsu Gakkai Zasshi.* 2013 Jul;69(7), 753–760.
- Koivisto J, Kiljunen T, Wolff J, Kortensniemi M. Assessment of effective radiation dose of an extremity CBCT, MSCT and conventional X-ray for knee area using MOSFET dosimeters. *Radiat Prot Dosimetry* 2013; 157: 515–24. doi: 10.1093/rpd/nct162
- Lavallée MC, Gingras L, Beaulieu L., “Energy and integrated dose dependence of MOSFET dosimeter sensitivity for irradiation energies between 30 kV and 60Co”, *Med. Phys.* 33, pp. 3683–3689, 2006.

- Lee R, Thomas KE, Connolly BL, Falkiner M, Gordon CL. Effective dose estimation for pediatric voiding cystourethrography using an anthropomorphic phantom set and metal oxide semiconductor field-effect transistor (MOSFET) technology. *Pediatr Radiol*. 2009 Jun;39(6):608-15.
- Lian CPL, Othman MAR, Cutajar D, Butson M, Guatelli S and Rosenfeld AB. Monte Carlo study of the energy response and depth dose water equivalence of the MOSkin radiation dosimeter at clinical kilovoltage photon energies. *Australas. Phys. Eng. Sci. Med.* 34(2), 273 – 279 (2011).
- Lian C, Wong J, Young A, Cutajar D, Petasecca M, Lrech M and Rosenfeld A. Measurement of multi- slice computed tomography dose profile with the dose magnifying glass and the MOSkin radiation dosimeter. *Radiation Measurements*, 2013, 55: 51–53.
- Lofthag-Hansen S, Thilander-Klang A, Ekestubbe A, Helmrot E and Gröndahl K. Calculating effective dose on a cone beam computed tomography device: 3D Accuitomo and Accuitomo FPD. *Dentomaxillofacial Radiology* 2008; 37: 72–79.
- Loubele M, Maes F, Jacobs R, van Steenberghe D, White SC, Suetens P. Comparative study of image quality for MSCT and CBCT scanners for dentomaxillofacial radiology applications. *Radiat Prot Dosimetry*. 2008;129(1–3):222-6.
- Loubele M, Bogaerts R, VanDijck E, Pauwels R, Vanheusden S, Suetens P, Marchal G, Sanderink G, Jacobs R. Comparison between effective radiation dose of CBCT and MSCT scanners for dentomaxillofacial applications. *Eur J Radiol*. 2009 Sep; 71(3): 461-8.
- Ludlow JB, Davies-Ludlow LE, Brooks SL. Dosimetry of two extraoral direct digital imaging devices: NewTom cone beam CT and Orthophos plus DS panoramic unit. *Dentomaxillofac Radiol* 2003;32:229-34.
- Ludlow JB, Brooks SL, Davies-Ludlow LE, Howerton B. Dosimetry of 3 CBCT units for oral and maxillofacial radiology. *Dentomaxillofac Radiol* 2006; 35:219-26.
- Ludlow JB, Ivanovic M. Comparative dosimetry of dental CBCT devices and 64-slice CT for oral and maxillofacial radiology. *Oral Surg Oral Med Oral Pathol Oral Radiol Endod* 2008;106:106-14.
- Ludlow JB. Dose and risk in dental diagnostic imaging: with emphasis on dosimetry of CBCT. *Korean Journal of Oral and Maxillofacial Radiology* 2009;39:175–184.
- Ludlow JB, Walker C. Assessment of phantom dosimetry and image quality of i-CAT FLX cone-beam computed tomography. *Am J Orthod Dentofacial Orthop*. 2013 Dec;144(6):802-17. doi: 10.1016/j.ajodo.2013.07.013.
- Ludlow JB, Timothy R, Walker C, Hunter R, Benavides E, Samuelson DB & Scheske MJ. (2014). Effective dose of dental CBCT—a meta analysis of published data and additional data for nine CBCT units. *Dentomaxillofacial Radiology*, 44(1).

- Manninen 2014a, Manninen AL, Kotiaho A, Nikkinen J and Nieminen MT Validation of a MOSFET Dosimeter System for Determining the Absorbed and Effective Radiation Doses in Diagnostic Radiology. *Radiation Protection Dosimetry* (2014), pp. 1–7
- Manninen 2014b, Manninen AL. (2014). *Clinical Applications of Radiophotoluminescence (RPL) Dosimetry in Evaluation of Patient Radiation Exposure in Radiology*. (Doctoral dissertation, Faculty of Medicine, University of Oulu, Finland)
- McCullough CH, Leng S, Yu L, Cody DD, Boone JM and McNitt-Gray MF. CT Dose Index and Patient Dose: They Are Not the Same Thing 2011 *Radiology*, 259, 311–316.
- Miksys N, Gordon CL, Thomas K, Connolly BL. Estimating effective dose to pediatric patients undergoing interventional radiology procedures using anthropomorphic phantoms and MOSFET dosimeters. *AJR Am J Roentgenol*. 2010 May;194(5):1315-22.
- Miracle AC, Mukherji SK. Conebeam CT of the Head and Neck, Part 2: Clinical Applications. *AJNR Am J Neuroradiol* 2009 Aug; 30(7):1285-92.
- Mitch MG, DeWerd LA, Minniti R, Williamson JF. Treatment of uncertainties in radiation dosimetry. In: *AAPM Summer Scholl*, July, 23, 2009.
- Mori S, Endo M, Nishizawa K, et al. Enlarged axial dose profiles in cone-beam CT and the need for modified dosimetry. *Med Phys*. 2005;32(4):1061–69.
- Mozzo P, Procacci C, Tacconi A, Martini PT, Andreis IA. A new volumetric CT machine for dental imaging based on the cone-beam technique: preliminary results. *Eur Radiol*. 1998;8(9):1558-64.
- NBS Handbook No. 85 1964, *Physical Aspects of Irradiation* (NBS Handbook No. 85. Washington DC: US Government Printing Office, Mar. 1964, p.3.
- NRPB, 1992, Institute of Physical Sciences in Medicine, National Radiological protection Board, College of Radiographers. *National Protocol for Patient Dose Measurements in Diagnostic Radiology*. Chilton: NRPB, 1992
- O’Connell B, Conneely C, McCarthy C, Doyle, J, Lane W, Adams L. “Electrical performance and radiation sensitivity of stacked PMOS dosimeters under bulk bias control”, *IEEE Trans. Nucl. Sci.*, Vol.45, Iss.6, 1998, pp. 2689–2694.
- Pauwels R, Beinsberger J, Collaert B, Theodorakou C, Rogers J, Walker A, et al. Effective dose range for dental cone beam computed tomography scanners. *Eur J Radiol*. 2012 Feb;81(2):267-71
- Pauwels R, Theodorakou C, Walker A, Bosmans H, Jacobs R, Horner K, et al. Dose distribution for dental cone beam CT and its implication for defining a dose index. *Dentomaxillofac Radiol*. 2012 Oct;41(7):583-93.
- Peet DJ and Pryor MD. Evaluation of a MOSFET radiation sensor for the measurement of entrance surface dose in diagnostic radiology, *Br J Radiol* 1999; 72:562–568

- Peet DJ, Pryor MD. Evaluation of a MOSFET radiation sensor for the measurement of entrance surface dose in diagnostic radiology. *Br J Radiol.* 1999 Jun;72(858):562-8.
- Podnieks EC, Negus IS. Practical patient dosimetry for partial rotation cone beam CT. *Br J Radiol.* 2012 Feb;85(1010):161-7.
- Preston DL, Ron E, tokuoka S, Funamoto S, Nishi N, Soda M, Mabuchi K, Kodama K. Solid cancer incidence in atomic bomb survivors: 1958–1998. *Radiat Res* 2007; 168: 1–64.
- Price RA, Benson C, Rodgers K, “Development of a RadFET linear array for intracavitary in vivo dosimetry in external beam radiotherapy and brachytherapy”, *IEEE Trans. Nucl. Sci.*, Vol. 51 No. 4, pp 1420–1426, 2004.
- Qu X, Gang L, Ludlow J B, Zu-yan Z, DDS, Xu-chen. Effective radiation dose of ProMax 3D cone-beam computerized tomography scanner with different dental protocols. *Oral Surgery, Oral Medicine, Oral Pathology, Oral Radiology and Endontology* 2010; Vol. 110 No.6.
- Ramaseshan R, Khli KS, Zhang TJ, Lam T, Nordlinger B, Hallil A, and Islam M, “Performance characteristics of a microMOSFET as an in vivo dosimeter in radiation therapy” *Phys. Med. Biol.* 49, pp. 4031- 4048, 2004.
- Robb RA, The Dynamic Spatial Reconstructor: An X-ray Video-Fluoroscopic CT Scanner for Dynamic Volume Imaging of Moving Organs. *IEEE Trans Med Imaging.* 1982;1(1):22-33.
- Roberts JA, Drage NA, Davies J, Thomas D W. Effective dose from cone beam CT examinations in dentistry. *British Journal of Radiology* (2009) 82, 35–40.
- Rottke D, Patzelt S, Poxleitner P, Schulze D. Effective dose span of ten different cone beam CT devices. *Dentomaxillofac Radiol.* 2013;42(7):20120417. doi: 10.1259/dmfr.20120417. Epub 2013 Apr 12.
- Roxby P, Foroudi F and Haworth A. Simple methods to reduce patient dose in a Varian cone beam CT system for delivery verification in pelvic British Journal of Radiology (2009) 82, 855–859© 2009 British Institute of Radiology doi: 10.1259/bjr/37579222.
- Sarrabayrouse G, Gessinn F, Thick oxide MOS transistors for ionizing radiation dose measurement, *Radioprotection* 1994 Vol. 29. n. 4, pp. 557–572
- Sarrabayrouse G, Buchdahl D, Polischuk V, Siskos S, “Stacked-MOS ionizing radiation dosimeters: potentials and limitations”, *Rad. Phys. and Chem.*, Vol. 71, No 3–4, pp. 737–739, 2004.
- Scarfe WC. Imaging of maxillofacial trauma: evolutions and emerging revolutions. *Oral Surg Oral Med Oral Pathol Oral Radiol Endod* 2005; **100**: S75–S96 (PMID: 16037795 DOI: 10.1016/j.tripleo.2005.05.057)
- Scarfe WC, Farman AG. Cone beam computed tomography: A paradigm shift for clinical dentistry. July/August 2007 *Australasian Dental Practice* 103

- Scarfe WC, Farman AG. What is Cone-Beam CT and How Does it Work? *Dent Clin N Am* 52 (2008) 707–730
- SEDENTEX 2011, PROTECTION, SEDENTEXCT-Radiation. Cone beam CT for dental and maxillofacial radiology. Provisional guidelines A report prepared by the SEDENTEXCT project. Version1.(cited 1-05-2009). Available from: URL:< <http://www.sedentext.eu>, 2011.
- Shope TB, Gagne RM, Johnson GC. A method for describing the doses delivered by transmission x-ray computed tomography. *Med Phys* 1981;8(4):488–495
- Soubra M and Cygler, Evaluation of dual bias dual metal oxide-silicon semiconductor field effect transistor detector as radiation dosimeter, *J. Am. Assoc. Phys. Med* 1994. p. 567–572.
- Spezi, E, Downes, P, Jarvis, R, Radu E, & Staffurth J. (2012). Patient-specific three-dimensional concomitant dose from cone beam computed tomography exposure in image-guided radiotherapy. *International Journal of Radiation Oncology* Biology* Physics*, 83(1), 419–426.
- Suomalainen A, Kiljunen T, Käser Y, Peltola J, Kortensniemi M. Dosimetry and image quality of four dental cone beam computed tomography scanners compared with multislice computed tomography scanners. *Dentomaxillofacial Radiology* 2009; 38:367–378.
- Suomalainen, A. (2010). *Cone beam computed tomography in oral radiology* (Doctoral dissertation, Faculty of Medicine, University of Helsinki).
- Tapiovaara M, Tapiovaara T. The validation and user's manual of the Spektripaja (2.0) program. Report STUK-TR 3. Helsinki: Radiation and Nuclear Safety Authority, 2008. (In Finnish)
- Tapiovaara M, Siiskonen T. PCXMC. A Monte Carlo program for calculating patient doses in medical x-ray examinations (2nd Ed.), Report STUK-A231. Helsinki, Finland: Radiation and Nuclear Safety Authority, 2008.
- Tarr NG, Mackay GF, Shortt K and Thomson I. A Floating Gate MOSFET Dosimeter Requiring No External Bias Supply, *IEEE TRANSACTIONS ON NUCLEAR SCIENCE*. VOL. 45. NO. 3. JUNE 1998
- Tarr G, Shortt K, Wang Y, Thomson I, “A Sensitive, Temperature- Compensated, Zero-Bias Floating Gate MOSFET Dosimeter”, *IEEE Trans. Nucl. Sci*. VOL. 51, NO. 3, pp.1277–1282, 2004.
- Thilander-Klang, A. and Helmrot, E. Methods of determining the effective dose in dental radiology. *Radiat. Prot. Dosim.* 139(1–3), 306–309 (2010).
- Toncheva G, Fredrickson M, Yoshizumi TT, “Variation of MOSFET calibration factor as a function of dosimeter age,” *Med. Phys.* 37, 3116–3117 (2010).
- Tsiklakis K, Donta C, Gavala S, Karayianni K, Kamenopoulou V, Hourdakos CJ. Dose reduction in maxillofacial imaging using low dose Cone Beam CT. *Eur J Radiol.* 2005 Dec;56(3):413-7.

- Vassileva J, Stoyanov D. Quality control and patient dosimetry in dental cone beam CT. *Radiat Prot Dosimetry*. 2010 Apr–May;139(1–3):310-2.
- Wallace M, Kuo M, Glaiberman C, Binkert C, Orth R, MD, Soulez G. Three-Dimensional C-arm Cone-beam CT: Applications in the Interventional Suite. *J Vasc Interv Radiol* 2008; 19:799–813
- Xu J, Reh DD, Carey JP, Mahesh M, Siewerdsen JH. Technical assessment of a cone-beam CT scanner for otolaryngology imaging: image quality, dose, and technique protocols. *Med Phys*. 2012 Aug;39(8):4932-42. doi: 10.1118/1.4736805.
- Yoshizumi TT, Goodman PC, Frush DP, EA. Validation of Metal Oxide Semiconductor Field Effect Transistor Technology for Organ Dose Assessment During CT: Comparison with Thermoluminescent Dosimetry. *AJR*: 188, May 2007.
- Yu L, Liu X, Leng S, Kofler JM, Ramirez-Giraldo JC, Qu M, et al. Radiation dose reduction in computed tomography: techniques and future perspective. *Imaging Med*. 2009 Oct;1(1):65–84.
- Yu L., Vrieze T. J., Bruesewitz M. R., Kofler J. M., DeLone D. R., Pallanch J. F., Lindell E. P. and McCollough C. H. Dose and Image Quality Evaluation of a Dedicated Cone-Beam CT System for High-Contrast Neurologic Applications *AJR*:194, February 2010.

PUBLICATION I

Koivisto J, Wolf J, Kiljunen T, Schulze D, Kortensniemi M.

“Characterization of MOSFET dosimeters for low-dose measurements in maxillofacial anthropomorphic phantoms”

J Appl Clin Med Phys. 2015 Jul 8;16(4):5433.

© 2015 Reston

Reprinted with permission

PUBLICATION II

Koivisto J, Kiljunen T, Wolf J, Kortensniemi M.

“Characterization of MOSFET dosimeter angular dependence in three rotational axes measured free-in-air and in soft-tissue equivalent material”.

Journal of Radiation Research, 2013, 00, 1–7 doi: 10.1093/jrr/rrt015

© 2013 Oxford University Press

Reprinted with permission

PUBLICATION III

Koivisto J, Kiljunen T, Tapiovaara M, Wolff J, Kortensniemi M.

“Assessment of radiation exposure in dental cone-beam computerized tomography with the use of metal-oxide semiconductor field-effect transistor (MOSFET) dosimeters and Monte Carlo simulations”.

Oral Surg Oral Med Oral Pathol Oral Radiol 2012;114:393-400

© 2012 Elsevier

Reprinted with permission

PUBLICATION IV

Koivisto J, Schulze D, Wolff J, Rottke D.

“Effective dose assessment in the “maxillofacial region using thermoluminescent (TLD) and metal oxide semiconductor field- effect transistor (MOSFET) doseimeters: a comparative study”.

**Dentomaxillofac Radiol. 2014;43(8):20140202. doi: 10.1259/
dmfr.20140202. Epub 2014 Aug 21.**

© 2014 BIR Publications
Reprinted with permission

PUBLICATION V

Koivisto J, Wolff J, Järnstedt J, Dastidar P, Kortesiemi M.

“Assessment of the effective dose in supine, prone, and oblique positions in the maxillofacial region using a novel combined extremity and maxillofacial cone beam computed tomography scanner.”

**Oral Surg Oral Med Oral Pathol Oral Radiol. 2014 Sep;118(3):355-62.
doi: 10.1016/j.oooo.2014.05.016. Epub 2014 Jun 14.**

© 2014 Elsevier

Reprinted with permission